

Developmental Cell

Small RNAs Are Trafficked from the Epididymis to Developing Mammalian Sperm

Highlights

- Detailed characterization of small RNA dynamics in mammalian sperm maturation
- Caput epididymosomes can deliver small RNAs to testicular spermatozoa *in vitro*
- Metabolic labeling of RNAs in intact animals tracks RNAs from epididymis to sperm

Authors

Upasna Sharma, Fengyun Sun, Colin C. Conine, ..., Veronika A. Herzog, Stefan L. Ameres, Oliver J. Rando

Correspondence

oliver.rando@umassmed.edu

In Brief

Recent studies suggest that sperm carry RNAs first synthesized in epididymal somatic cells. Sharma et al. test this hypothesis, characterizing small RNA population dynamics during sperm maturation. They show that caput epididymosomes can deliver RNAs to immature sperm *in vitro* and track RNAs *in vivo* from the epididymis to sperm using metabolic labeling.

Small RNAs Are Trafficked from the Epididymis to Developing Mammalian Sperm

Upasna Sharma,¹ Fengyun Sun,¹ Colin C. Conine,¹ Brian Reichholf,² Shweta Kukreja,¹ Veronika A. Herzog,² Stefan L. Ameres,² and Oliver J. Rando^{1,3,*}

¹Department of Biochemistry and Molecular Pharmacology, University of Massachusetts Medical School, Worcester, MA 01605, USA

²Institute of Molecular Biotechnology (IMBA), Vienna Biocenter Campus (VBC), 1030 Vienna, Austria

³Lead Contact

*Correspondence: oliver.rando@umassmed.edu

<https://doi.org/10.1016/j.devcel.2018.06.023>

SUMMARY

The biogenesis of the RNA payload of mature sperm is of great interest, because RNAs delivered to the zygote at fertilization can affect early development. Here, we tested the hypothesis that small RNAs are trafficked to mammalian sperm during the process of post-testicular maturation in the epididymis. By characterizing small RNA dynamics during germ cell maturation in mice, we confirm and extend prior observations that sperm undergo a dramatic switch in the RNA payload from piRNAs to tRNA fragments (tRFs) upon exiting the testis and entering the epididymis. Small RNA delivery to sperm could be recapitulated *in vitro* by incubating testicular spermatozoa with caput epididymosomes. Finally, tissue-specific metabolic labeling of RNAs in intact mice definitively shows that mature sperm carry RNAs that were originally synthesized in the epididymal epithelium. These data demonstrate that soma-germline RNA transfer occurs in male mammals, most likely via vesicular transport from the epididymis to maturing sperm.

INTRODUCTION

Inheritance of phenotypic changes in the absence of any change in DNA is known as epigenetic inheritance and is essential for cell state inheritance during mitosis. Epigenetic information is not only inherited during cell division—as at least some epigenetic information can be transmitted from one generation to the next in multicellular organisms—a mechanistically complex process that requires epigenetic information to be maintained throughout the disruptive processes of gametogenesis, fertilization, and early embryonic development. Although decades of study of cell state inheritance and other cases of epigenetic inheritance have identified several major molecular conduits of epigenetic information—chromatin structure, small RNAs, DNA modifications, prions, and transcription factors—much remains to be understood regarding the establishment and erasure of epigenetic information during gametogenesis and early development.

Small (<40 nt) RNAs are one of the best established carriers of epigenetic information and play key roles in epigenetic inheritance paradigms in *Caenorhabditis elegans* (Fire et al., 1998), *Arabidopsis thaliana* (Arteaga-Vazquez and Chandler, 2010; Hamilton and Baulcombe, 1999; Zilberman et al., 2003), *Schizosaccharomyces pombe* (Volpe et al., 2002), *Drosophila melanogaster* (Brennecke et al., 2008; de Vanssay et al., 2012), and mammals (Chen et al., 2016a; Gapp et al., 2014; Rassoulzadegan et al., 2006; Rodgers et al., 2015; Sharma et al., 2016). Multiple distinct families of small RNAs have been described that differ from one another in their biogenesis and in their regulatory functions and include well-studied species such as microRNAs, endo-siRNAs, and the germline-enriched class of piRNAs, which are crucial for self-nonsel recognition during gametogenesis (Aravin et al., 2006; Batista et al., 2008; Brennecke et al., 2007; Mochizuki et al., 2002; Shirayama et al., 2012; Vagin et al., 2006). In addition, a number of less-studied small RNA species have been described, including cleavage products of various noncoding RNAs including tRNAs—these latter RNAs are commonly referred to as tRNA fragments or “tRFs” (Anderson and Ivanov, 2014; Lee et al., 2009; Sobala and Hutvagner, 2011). Although tRFs have been found in numerous small RNA sequencing datasets, they seem to be particularly abundant in contexts related to reproduction, as for example 3' tRFs are the primary cargo of the *Tetrahymena* Piwi-related argonaute Tiwi12 (Couvillion et al., 2010), whereas 5' tRFs comprise the vast majority (~80%) of readily cloned small RNAs in mature mammalian sperm (Chen et al., 2016a; García-López et al., 2014; Peng et al., 2012; Rompala et al., 2018; Sharma et al., 2016).

The mechanisms responsible for the biogenesis of the small RNA payload of mammalian sperm are not completely understood. Small RNA dynamics have been extensively studied during the process of testicular spermatogenesis, where three Piwi-clade argonaute proteins (MIWI, MILI, and MIWI2) orchestrate two major waves of piRNA biosynthesis (Aravin et al., 2006; Aravin et al., 2007; Kuramochi-Miyagawa et al., 2004; Li et al., 2013). Initially, “pre-pachytene” piRNAs—primarily derived from repeat elements—are expressed beginning in spermatogonia (Aravin et al., 2007), followed by a wave of unique pachytene piRNAs, which are processed from 214 long noncoding precursor transcripts (Li et al., 2013). Given that the small RNAs found in testes are almost entirely comprised of piRNAs, it is noteworthy that the vast majority of small RNAs present in mature fertilization-competent sperm are tRFs. Indeed, tRFs

are vanishingly scarce (~2% of all small RNAs) in intact testes (Peng et al., 2012; Sharma et al., 2016), despite the fact that testes are primarily comprised of gametes at varying stages of development, which raises the broader question of how and when small RNAs are gained or lost during post-testicular maturation.

We recently uncovered a potential role for the epididymis—a long convoluted tubular structure where mammalian sperm undergo post-testicular maturation—in modulating the small RNA repertoire of maturing sperm (Sharma et al., 2016). We found that tRNA cleavage occurs robustly in the epididymis and that small vesicles secreted by the epididymal epithelium, known as epididymosomes (Belleannée et al., 2013; Krapf et al., 2012; Sullivan et al., 2007; Sullivan and Saez, 2013), carry a very similar population of small RNAs to that gained by sperm during epididymal transit (Sharma et al., 2016). Moreover, as sperm successively pass from caput (proximal) to cauda (distal) epididymis, sperm gain specific small RNAs that are locally enriched in the underlying epithelium. Finally, we and others (Reilly et al., 2016) have shown that epididymosomes can deliver small RNAs to relatively immature caput epididymal sperm *in vitro*, suggesting that the sperm small RNA repertoire is shaped by soma-to-germline trafficking of small RNAs.

Here, we rigorously test this hypothesis, characterizing developmental dynamics of small RNAs across multiple purified sperm populations, spanning testicular and post-testicular development. We detected very low levels of tRFs in all testicular germ cell populations, including mature testicular spermatozoa, which confirmed that tRFs are only gained upon entry into the epididymis. This maturation step could be partially recapitulated *in vitro*, as we show that epididymosomes from the proximal epididymis can deliver a wide variety of small RNAs, including both microRNAs and tRFs, to testicular spermatozoa. Finally, we use a chemogenetic approach to definitively identify the tissue of origin for small RNAs present in mature cauda epididymal sperm. Using an epididymis-specific expression of uracil phosphoribosyltransferase (UPRT) to enable 4-thiouracil labeling of small RNAs synthesized in the caput epididymis, we show that mature cauda sperm carry small RNAs that are first synthesized in the epididymis epithelium. Taken together, these data demonstrate that small RNAs are trafficked from soma to germline in mammals and provide further evidence that the small RNA payload of mature sperm is shaped by successive waves of epididymosomal delivery during the post-testicular maturation process.

RESULTS

Improved Characterization of the Small RNA Contents of Mouse Sperm

Increasing interest in the potential for sperm RNAs to serve regulatory functions in the early embryo has motivated a number of groups to characterize the mammalian sperm RNA payload via deep sequencing methods. Although many studies yield similar findings—with 5' tRFs representing the vast majority (~80%) of sperm small RNAs (Chen et al., 2016a; García-López et al., 2014; Peng et al., 2012; Rompala et al., 2018; Sharma et al., 2016; Yang et al., 2016)—there is nonetheless substantial variation between studies, some of which report significantly lower

tRF levels (de Castro Barbosa et al., 2016; Kawano et al., 2012). Beyond trivial protocol differences such as the size range of purified RNAs, RNA recovery depends on many additional factors, ranging from the purity of the sperm preparation to the effects of nucleotide modifications on RNA adaptor ligation or cloning. We therefore sought to characterize the effects of several protocol steps—sperm washing, sperm head and tail separation, RNA isolation, and enzyme treatments—on the recovery of 18–40 nt small RNAs from murine sperm samples. As the sperm small RNA payload is dramatically remodeled at the transition from testicular spermatogenesis to post-testicular sperm maturation in the epididymis, we characterized the effects of key protocol steps not only on RNA recovery from the tRF-dominated payload of mature cauda sperm but also on the recovery of the piRNA-dominated cargo of selected testicular sperm populations. Overall, we assessed the RNA contents of six germ cell populations obtained from throughout the reproductive tract of sexually mature (8- to 12-week-old) male mice, as well as intact testis and cauda epididymis. Sperm populations included mature sperm obtained from caput and cauda epididymis, primary spermatocytes, two fractions of round spermatids (Sharma et al., 2016), and a previously unsequenced population of testicular spermatozoa purified using Percoll gradients (STAR Methods and Figure S1A).

First, given that sperm samples are typically washed following isolation from epididymal contents, we asked how different wash conditions affect small RNA recovery. The 10- to 12-week-old male mice were sacrificed, and the cauda epididymis was dissected with cuts to the corpus epididymis and vas deferens immediately adjacent to the bulk of the cauda. Epididymal contents were gently squeezed out into tissue culture media, and sperm from four animals were pooled, gently pelleted and washed with PBS, and split into four aliquots: one aliquot was immediately pelleted for RNA isolation, and the other three were subjected to low, medium, or high stringency detergent washes (Figures S1B and S1C; STAR Methods). Total RNA was extracted, and 18–40 nt small RNAs were gel-purified and cloned using the Illumina TruSeq protocol. Overall, we find similar RNAs captured consistently across all four samples, with 5' tRFs representing the most abundant RNA species in all four datasets (Table S1). Relative to unwashed sperm, any detergent washing step resulted in a decreased overall abundance of microRNAs, resulting from a loss of a specific subset of microRNAs such as let-7 family members (Figures S1B and S1C). This presumably reflects the removal of excess adherent epididymosomes or ribonucleoprotein complexes from the surface of sperm—indeed, the specific microRNAs lost after washing include species that are particularly abundant in partially purified epididymosome preparations relative to sperm (Sharma et al., 2016). After higher-stringency washing, we obtained lower levels of rRNA fragments and small nucleolar RNA (snoRNA) fragments, potentially resulting from the permeabilization of sperm and the loss of cytoplasmic contents. Indeed, while sperm largely remained intact following the low stringency washes, we observed that sperm washed at the intermediate stringency were often broken into head and tail sections (not shown), consistent with these conditions possibly disrupting the sperm membrane. Overall, these analyses demonstrate that overall RNA recovery is not greatly affected by the washing protocol but suggest that a low

stringency detergent wash should be used to remove adherent material from the sperm surface to provide the most reproducible results between different investigators.

We next investigated the subcellular localization of various small RNAs, separating sperm into heads and tails by sonication followed by sucrose gradient fractionation (Figure 1A). Small RNA profiles were broadly similar between heads and tails (Figure 1B), with a few notable differences for cauda sperm samples. Most dramatically, we find that piRNAs are highly enriched (~5-fold) in the tail preparations, consistent with the fact that remnants of the chromatoid body, central to piRNA biogenesis, localize to the sperm midpiece during sperm maturation (de Mateo and Sassone-Corsi, 2014; Meikar et al., 2011). More surprisingly, microRNAs are also generally enriched in tails relative to sperm heads, although this enrichment is less dramatic than that observed for piRNAs. Other RNA classes exhibited modest preferences for the head vs. tail—tRFs were overall moderately (~1.5-fold) enriched in sperm heads (Schuster et al., 2016), but a handful of specific tRFs (notably tRF-Gly-TCC) were relatively more abundant in tails (Table S2). As intracytoplasmic sperm injection (ICSI)—used in humans for a subset of assisted reproduction cases—typically involves the injection of a sperm head only into the oocyte, the differences documented here should motivate further investigation into the potential impacts of ICSI on pre-implantation development.

Finally, we noted that in several biological systems, tRNAs are cleaved by nucleases of the RNase A and T families (Andersen and Collins, 2012; Emará et al., 2010; Lee and Collins, 2005; Yamasaki et al., 2009), which are known to leave either 2'-3' cyclic phosphate or 3' phosphate moieties at the end of the 5' fragment, both of which can interfere with small RNA cloning protocols. We therefore repeated our characterization of sperm small RNAs following treatment with T4 Polynucleotide Kinase (PNK) in the absence of ATP, which resolves 2'-3' cyclic phosphates left at the 3' end of RNaseA and RNaseT family cleavage products (Figure 1C). PNK treatment of all samples tested—intact testis, cauda epididymis, caput sperm, and cauda sperm—resulted in a dramatic increase in rRNA-mapping reads (Figure S2A and Table S3). In addition, for all samples with the exception of the piRNA-dominated testes, PNK treatment revealed a previously unappreciated population of tRFs, with 5' tRFs becoming 2- to 4-fold more abundant (normalized relative to all non-rRNA reads) in PNK-treated epididymis RNA samples (Figure 1D and Figure S2B). Furthermore, PNK treatment resulted in a shift in the RNA length distribution to longer species (Figure 1E). Closer inspection of tRNA-mapping reads in these libraries revealed two new entities, both mapping to tRNA 5' ends. For most tRFs, PNK treatment revealed a population of slightly larger (~33–36 nt) tRNA cleavage products than the predominant ~28–32 nt species observed in no-PNK libraries, with this new population typically resulting from cleavage within or immediately adjacent to the anticodon (Figure 1F). For a smaller subset of tRNAs, we observed ~19–22 nt RNAs representing D-loop cleavage that are extremely scarce in no-PNK libraries (as shown for tRNA-Leu-CAG, Figure 1F). These data reveal what are presumably initial cleavage events for an RNaseA or RNaseT family nuclease at accessible tRNA loop structures, with the previously described shorter 28–32 nt fragments representing secondary degradation or trimming products.

Together, our data provide a more detailed picture of small RNA populations in the male reproductive tract and in sperm and provide experimental guidance for studies on environmental effects on the germline epigenome.

Small RNA Dynamics during Sperm Development and Maturation

Having a clearer picture of the small RNA populations present in mature sperm, we next turned to the dynamics of small RNA biogenesis during sperm development and maturation. As noted in the Introduction, sperm isolated from either the cauda (distal) or caput (proximal) epididymis carry a small RNA payload comprised primarily of tRFs. In contrast, tRNA cleavage as assayed both by small RNA sequencing and by northern blot is nearly undetectable in intact testes, where the vast majority of small RNAs are piRNAs (Peng et al., 2012; Sharma et al., 2016). Although these data suggest that tRFs are gained upon entry into epididymis, it remains formally possible that tRFs are gained during the last stages of testicular spermiogenesis as round spermatids mature into testicular spermatozoa.

Analysis of the small RNA payload of six germ cell populations—primary spermatocytes, two round spermatid populations, testicular spermatozoa (Figure S1A), and caput and cauda epididymal sperm—recapitulates prior findings, with piRNAs dominating the small RNA repertoire of spermatocytes and round spermatids and tRFs being the primary small RNA population in both caput and cauda epididymal sperm (Figure 2A and Table S4). Turning to the previously unexamined testicular spermatozoa, we find that even at this late stage of maturation, these sperm resemble other testicular populations rather than epididymal sperm—they continue to carry high levels of piRNAs (~80% of small RNA reads), having yet to gain abundant tRFs (~5% of reads). The RNA payload of mammalian sperm therefore shifts from piRNAs to tRFs at some point after sperm exit the testis for the epididymis.

In principle, the apparent gain of tRFs in epididymal sperm could simply result from the massive loss of piRNAs, leaving behind only the previously rare population of tRFs. To distinguish between “degradation only” and “degradation plus tRF gain” models, we spiked in several exogenous small RNAs at defined concentrations per sperm and deep sequenced testicular and caput sperm small RNAs. We consistently find a ~2-fold decrease in overall RNA levels as testicular sperm enter the epididymis (Figure S3), which cannot explain the ~10-fold enrichment of tRFs in caput sperm. In addition, other sperm small RNAs (such as microRNAs) do not change in abundance at a similar scale as tRFs, again arguing that piRNA degradation alone cannot explain changes in RNA contents as sperm enter the epididymis. Finally, we confirm that cauda sperm gain tRFs relative to testicular sperm by qRT-PCR, using U6 ncRNA (Nixon et al., 2015) as an internal control (Figure 2B). Together, our results are consistent with a “piRNA degradation plus tRF gain” model for the dramatic remodeling of sperm small RNA payload during epididymal maturation.

In addition to the bulk differences in abundance of broad classes of small RNAs, we also find marked differences in specific individual RNA species present in each germ cell population, confirming, for example, the previously described gain in tRF-Val-CAC that occurs as sperm transit from the caput to cauda

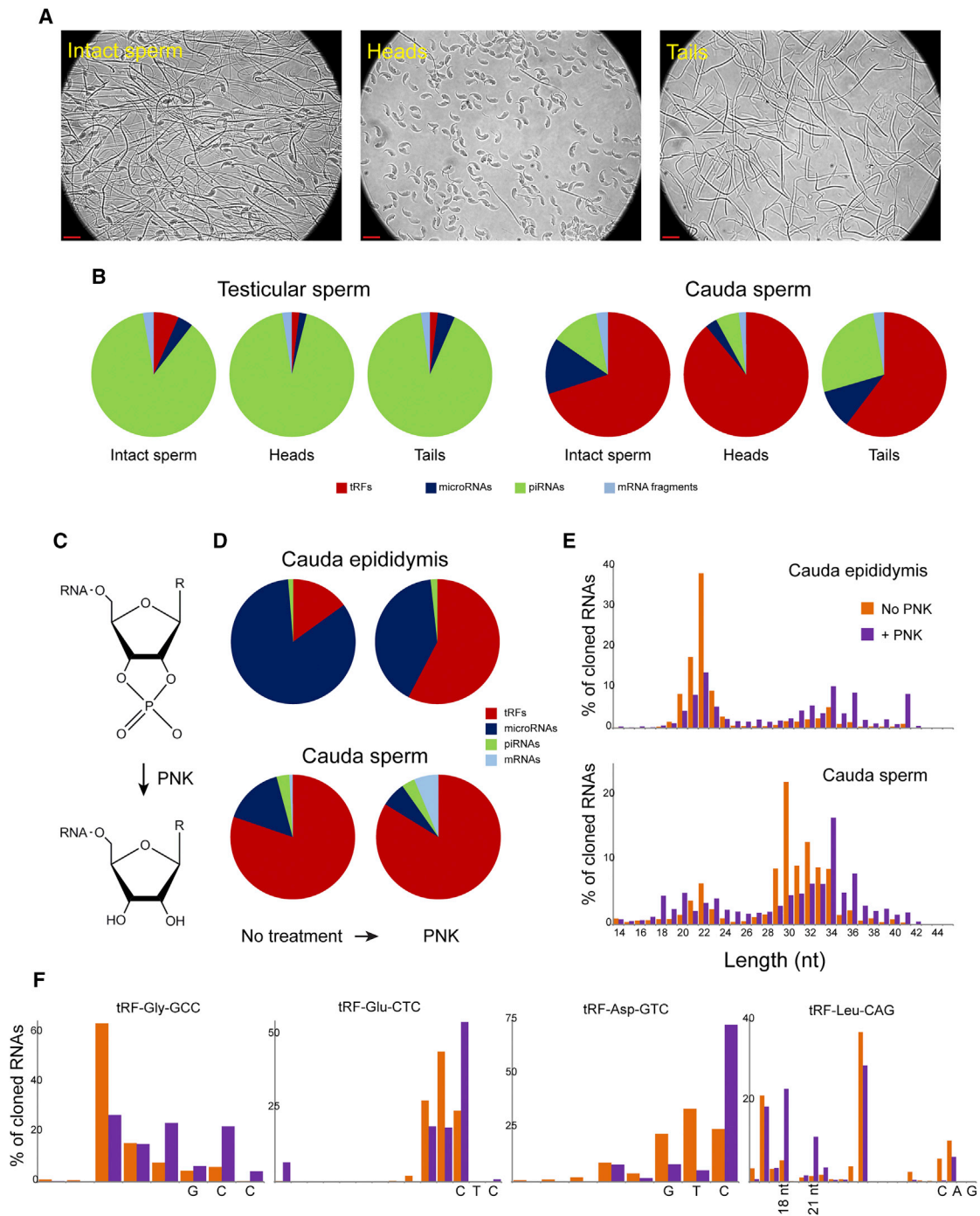


Figure 1. Subcellular Localization and 3' End Modifications of Sperm RNAs

(A) Separation of sperm into head- and tail-enriched fractions. Representative images of cauda epididymal sperm, showing intact sperm (left), along with head- and tail-enriched fractions, as indicated. Note that head and tail fractions are highly enriched but are not completely pure, as occasional sperm tails can be appreciated in the head preparation. Red scale bar represents 10 μ m.

(B) Subcellular fractionation of sperm small RNAs. Coarse differences between sperm head and tail preparations are shown for testicular sperm and cauda epididymal sperm. Pie charts show small RNA populations for sperm heads and tails, along with “intact sperm,” which have been sonicated for head versus tail separation but not separated. Notable here is the enrichment of piRNAs and microRNAs in the tails of cauda sperm, in contrast to the tRNA fragment enrichment in sperm heads.

(C) Resolution of cyclic 2'-3' phosphates by the phosphatase activity of polynucleotide kinase (PNK).

(D) Effects of PNK treatment on the recovery of major small RNA populations from cauda epididymis or cauda sperm.

(legend continued on next page)

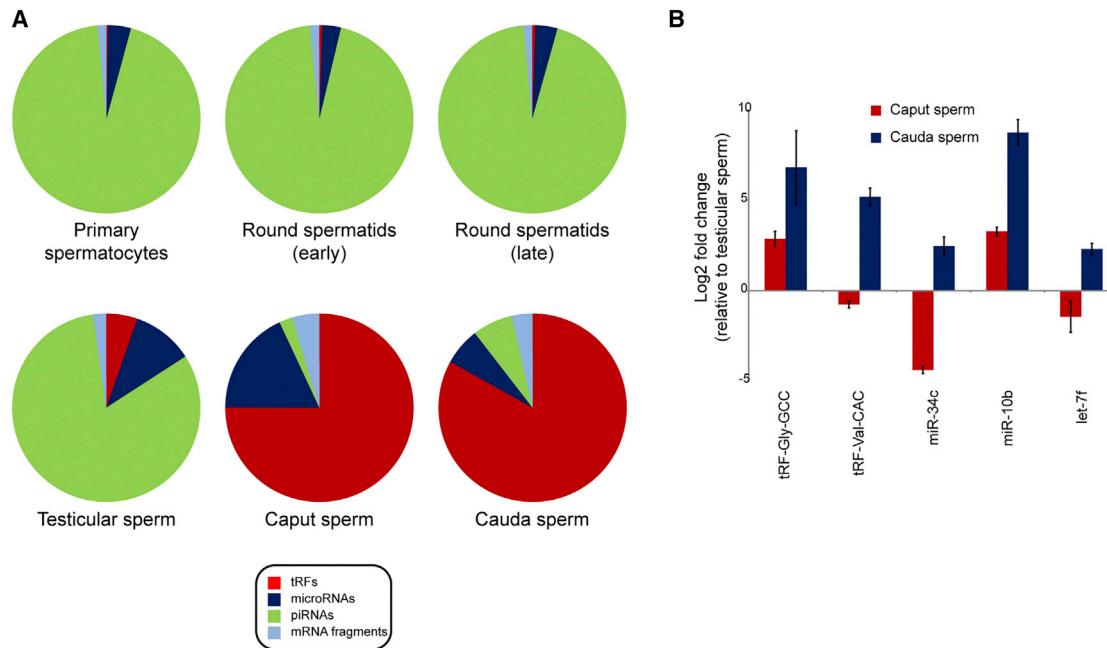


Figure 2. Bulk Small RNA Dynamics across Sperm Development

(A) Bulk changes to the small RNA payload throughout testicular and post-testicular sperm development. Pie charts are shown as in Figure 1B. For these six germ cell populations, small RNAs were cloned without PNK treatment, as PNK essentially had no effect on testicular RNA populations beyond increasing the fraction of rRNA-mapping reads (Figure S2A).

(B) Validation of deep sequencing data by qRT-PCR. Using U6 ncRNA as a normalization control, we assayed the levels of the indicated small RNAs in triplicate samples of testicular sperm, caput sperm, and cauda sperm. Bars show U6-normalized changes in small RNA abundance (y axis, log₂ scale) relative to testicular sperm. These data confirm the gain of tRFs observed in epididymal sperm relative to testicular sperm, as well as the strong cauda-specific enrichment for tRF-Val-CAC. miR-10b also exhibits a dramatic gain in the epididymis observed in deep sequencing data, while the surprising loss of miR-34c in caput sperm followed by its restoration in cauda sperm is also confirmed. In contrast, let-7f levels are relatively stable across sperm maturation.

epididymis (Sharma et al., 2016). In contrast to the highly tissue-restricted expression of piRNAs and tRFs, individual microRNAs exhibit more diverse behaviors during spermatogenesis and sperm maturation. To investigate microRNA dynamics in more detail, we re-normalized microRNA abundances according to total microRNA levels for each sperm population, rather than to all small RNAs, to avoid the confounding normalization effects of bulk piRNA loss and tRF gain. This analysis revealed a range of dynamic behaviors of individual microRNAs, ranging from relatively stable microRNAs such as let-7a and miR-181a/b, to microRNAs exhibiting dramatic changes in abundance throughout development (Figure 3). Many microRNAs were relatively rare in testicular sperm populations and then gained upon entry into the epididymis, with miR-21a, miR-29c, miR-199a, miR-200b/c, miR-10a/b, and many others, dramatically increasing in relative abundance during epididymal maturation. This is consistent with these RNAs potentially being trafficked to epididymal sperm alongside the bulk delivery of tRFs (Reilly et al., 2016; Sharma et al., 2016).

The contrasting behavior, with microRNAs expressed during testicular spermatogenesis being lost or diluted at later develop-

mental stages, was also common. Interestingly, for a surprisingly large subset of these microRNAs, the decrease in abundance observed in caput sperm was at least partially reversed later in the epididymis. In these cases, the microRNAs in question are abundant in testicular sperm as well as in cauda sperm but are scarce specifically in caput sperm. Interestingly, the majority of such microRNAs originate from genomic microRNA clusters of various sizes, ranging from small clusters (miR-15/16, the “oncomiR” 17-92 cluster, etc.) up to the megabase-scale imprinted X-linked miR-880 cluster. The changes in abundance of these microRNAs can be quite dramatic—many members of the miR-880 cluster (miR-871, miR-465c) are present at ~500 reads per million (across all small RNAs, not just microRNAs) in all four testicular germ cell populations, dropping to ~25 ppm in caput sperm before rebounding to ~400 ppm in cauda sperm. These changes in abundance cannot be explained by global changes in sperm RNA contents, and U6-normalized qRT-PCR (Figure 2B) confirmed the caput-specific loss of miR-34c observed in the deep sequencing dataset. Instead, this behavior is most consistent with these microRNAs initially being lost (by degradation or cytoplasmic elimination) upon epididymal entry,

(E) PNK treatment results in a shift toward longer RNA inserts in small RNA-Seq data. Data are shown for cauda epididymis and cauda sperm.

(F) Effects of PNK treatment on the lengths of 5' fragments of specific tRNAs, as indicated. Data are shown for cauda sperm RNAs—similar behavior was observed for cauda epididymis and caput sperm tRFs. For each tRNA, the three anticodon nucleotides are indicated on the x axis. See also Figures S1 and S2.

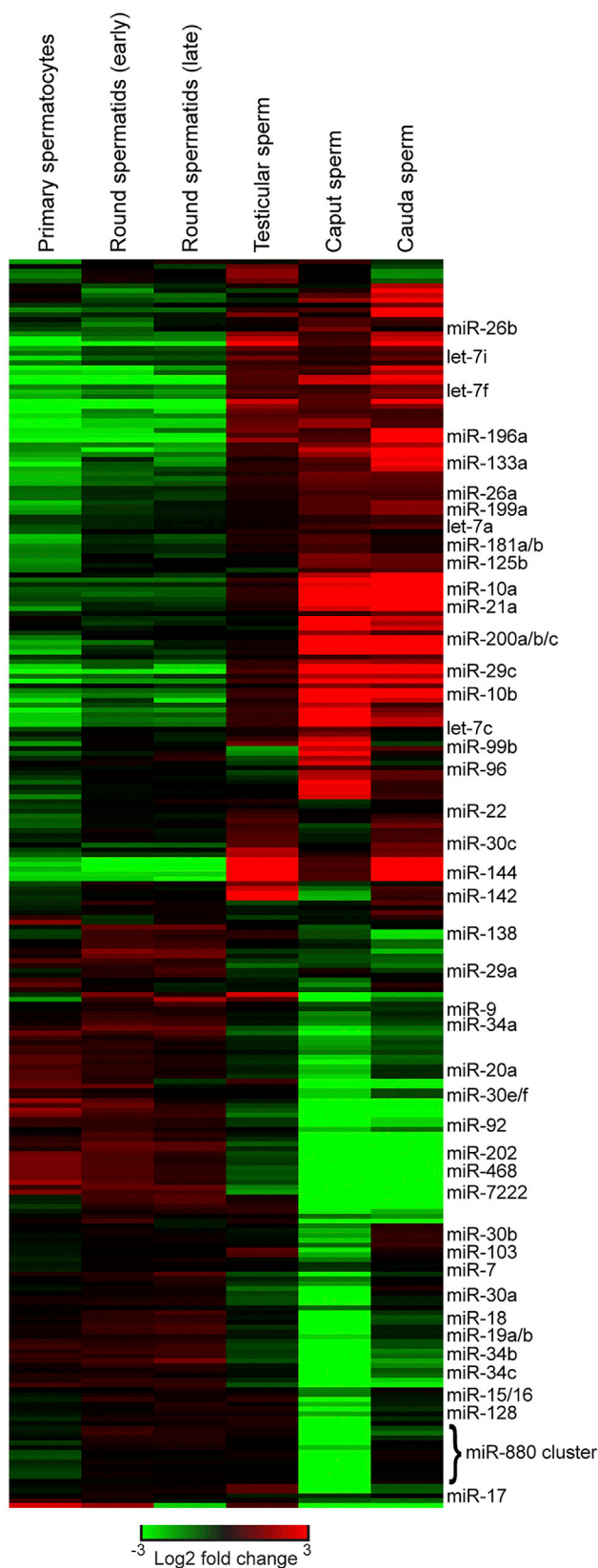


Figure 3. MicroRNA Dynamics across Sperm Development

MicroRNA abundances for all six germ cell populations were re-normalized only to the total microRNAs at a given developmental stage, then zero-centered for each row according to the median abundance across the six stages analyzed.

followed by a second load of these miRNAs either being generated *in situ* in cauda sperm from their precursor molecules, or shipped from epididymis epithelium to maturing sperm by epididymosomes. Consistent with the latter hypothesis, many of the microRNAs that are specifically scarce in caput sperm are abundant in cauda epididymosomes (Table S4). These data thus uncover surprisingly complex small RNA dynamics during sperm development and further underscore the major role of epididymal transit in the modulation of the sperm epigenome.

Caput Epididymosomes Deliver Small RNAs to Testicular Spermatozoa

Our data confirm and extend prior reports showing major differences between the small RNAs generated during testicular spermatogenesis and those gained during epididymal transit. What is the mechanism by which tRFs and other small RNAs are gained as sperm enter the epididymis? We previously showed that epididymosomes secreted by the epithelium of cauda epididymis have a similar RNA payload to that of mature sperm, and we and others have shown that epididymosomes can deliver small RNAs to relatively “immature” caput sperm (Reilly et al., 2016; Sharma et al., 2016). However, as the RNA repertoire of caput sperm is not particularly distinct from that of cauda sperm—caput sperm already carry high levels of most tRFs, for example—these reconstitution studies could focus only on a small handful of fairly cauda-specific species such as tRF-Val-CAC. In contrast, the RNA payload of testicular spermatozoa, which is dominated by piRNAs, is highly distinct from that of either epididymal sperm population, providing us with a relatively blank slate to more broadly explore the ability of epididymosomes to deliver RNAs to immature sperm.

Testicular sperm were isolated and then either mock-treated or incubated for 2 hr with caput epididymosomes, and resulting sperm were extensively washed to remove any contaminating vesicles (Figure 4A). We first used TaqMan qRT-PCR to assay two prominent tRFs present in epididymosomes but scarce in testicular sperm, which led to us finding that epididymosomal delivery results in a ~4- to 10-fold increase in abundance for these two tRFs (Figure 4B). To more broadly interrogate epididymosomal RNA delivery to sperm, we next carried out deep sequencing of small RNAs from mock and “reconstituted” sperm. Globally, we observed significantly higher levels of tRFs and microRNAs in reconstituted spermatozoa, relative to mock-treated sperm (Figures 4C and Table S5). Although 2-hr incubation is clearly insufficient to fully establish the caput small RNA payload, this is perhaps unsurprising given that purified caput sperm from intact animals have spent up to several days undergoing this delivery process.

More granular analysis of specific small RNA species revealed that the vast majority of piRNAs were unaffected by epididymosomal fusion (Figures 4D and 4E), consistent with the fact that piRNAs are expressed during testicular spermatogenesis and are largely absent from epididymosomes (and indicating that

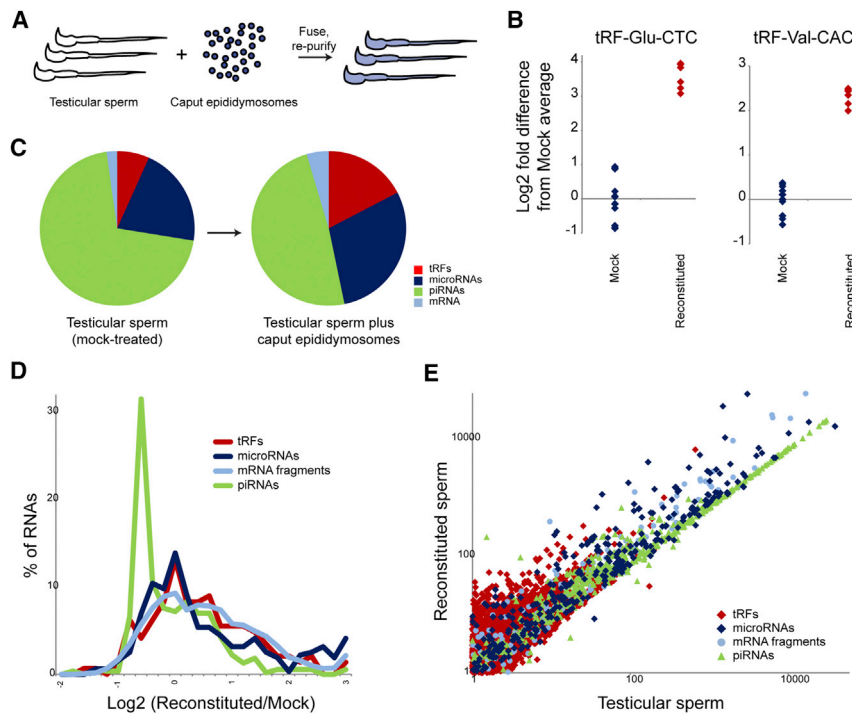


Figure 4. Reconstitution of Small RNA Delivery to Testicular Sperm

(A) Experimental schematic. Purified testicular sperm, which carry extremely low levels of tRFs, were incubated with caput epididymosomes for 2 hr, followed by extensive washing. Small RNAs were purified from either mock-treated testicular sperm or reconstituted sperm and analyzed either by qRT-PCR or deep sequencing.

(B) Delivery of two prominent tRFs to testicular sperm. TaqMan qRT-PCR for the indicated tRFs, with individual replicates plotted (on a \log_2 y axis) relative to the average level for mock-treated testicular sperm.

(C) Deep sequencing of testicular sperm either mock-treated or incubated with caput epididymosomes. Pie charts show average levels of various small RNA classes, revealing increased levels of microRNAs and tRFs delivered to testicular sperm by epididymosomes.

(D) Distribution of small RNA changes in sperm following epididymosome fusion. The x axis shows the \log_2 -fold difference between reconstituted and mock-treated sperm—positive values indicate delivery by epididymosomes. Importantly, because genome-wide normalization methods assume no global change in RNA abundance, RNAs that are in fact unaltered in the face of an overall gain of RNAs will exhibit a decrease in *relative*

abundance, as observed here for the bulk of piRNAs (average \log_2 -fold decrease of ~ 0.6). Values over -0.6 therefore indicate a gain of RNA during the fusion protocol.

(E) Scatterplot of small RNA abundances from deep sequencing data. The strong diagonal for piRNAs indicates the presence of RNAs in testicular sperm that are not affected by the delivery process. Note that essentially all RNAs here either lie along this diagonal, indicating that they are either absent or nearly so in caput epididymosomes, or above the diagonal, indicating widespread delivery of many RNA species to testicular sperm during reconstitution.

epididymosomal fusion does not induce piRNA degradation). This is clearly visualized in the scatterplot in Figure 4E, where piRNA abundance is strongly correlated between mock-treated and reconstituted sperm samples. Globally, nearly all small RNAs fall either on the same diagonal as the piRNAs—meaning that they are unaffected by epididymosomal fusion—or above this diagonal, consistent with delivery by epididymosomes. Individual tRFs and microRNAs exhibited a range of behaviors (Figures 4D and 4E), ranging from those unaffected by epididymosomal incubation and which are generally already abundant in testicular sperm and/or absent from caput epididymosomes, to efficiently delivered small RNAs that are highly abundant in caput epididymosomes (such as miR-10a/b, miR-148, miR-143, tRF-Glu-CTC, tRF-Gly-GCC, and tRF-His-GTG [Table S5]).

These data show that caput epididymosomes are capable of fusing with mature testicular spermatozoa to deliver their small RNA cargo *in vitro*, and, together with the *in vivo* small RNA dynamics detailed above, are most consistent with a mechanism of RNA biogenesis in mammalian sperm where small RNAs generated in the epididymis are trafficked to sperm in epididymosomes.

Chemogenetic Tracking of Small RNAs from Epididymis to Sperm

Although multiple observations here and elsewhere are most readily explained by the hypothesis that small RNAs in mature sperm are first generated in the epididymal epithelium, they do

not formally rule out the possibility that the small RNAs gained by sperm during epididymal maturation in intact animals are instead processed *in situ* from precursor molecules first synthesized during testicular spermatogenesis. In order to distinguish between these possibilities, we made use of the “TU tracer” mouse (Gay et al., 2013), in which tissue-specific expression of Cre recombinase is used to drive the expression of UPRT (Figure 5A). The expression of UPRT allows cells to incorporate 4-thiouracil (4-TU) into newly synthesized RNAs, thereby enabling tissue-specific metabolic labeling of RNA.

To assess the efficiency and specificity of this system, we first generated mice expressing UPRT specifically in the liver by mating *Albumin-Cre* (*Alb-Cre*) mice with TU-tracer mice. Cre-mediated recombination was extremely efficient, with nearly quantitative deletion of the GFP insert and concomitant expression of UPRT (Figures 5B and S4A)—remaining GFP likely reflects non-hepatocyte cell populations, such as blood cells, present in the liver. The resultant mice expressed UPRT specifically in liver, and injection of 4-TU in these mice resulted in the liver-specific labeling of RNAs, with undetectable background incorporation in other tissues (Figures 5C and 5D). Northern blot of labeled RNAs revealed 4-TU labeling of a wide range of RNA species including microRNAs (see below), but tRNAs and rRNAs were not efficiently labeled (not shown), either due to the poor use of 4-TU by PolI and PolIII or due to checkpointing of these typically highly modified RNAs. This protocol therefore enables us to characterize microRNA trafficking *in vivo* but unfortunately cannot be used to track tRFs.

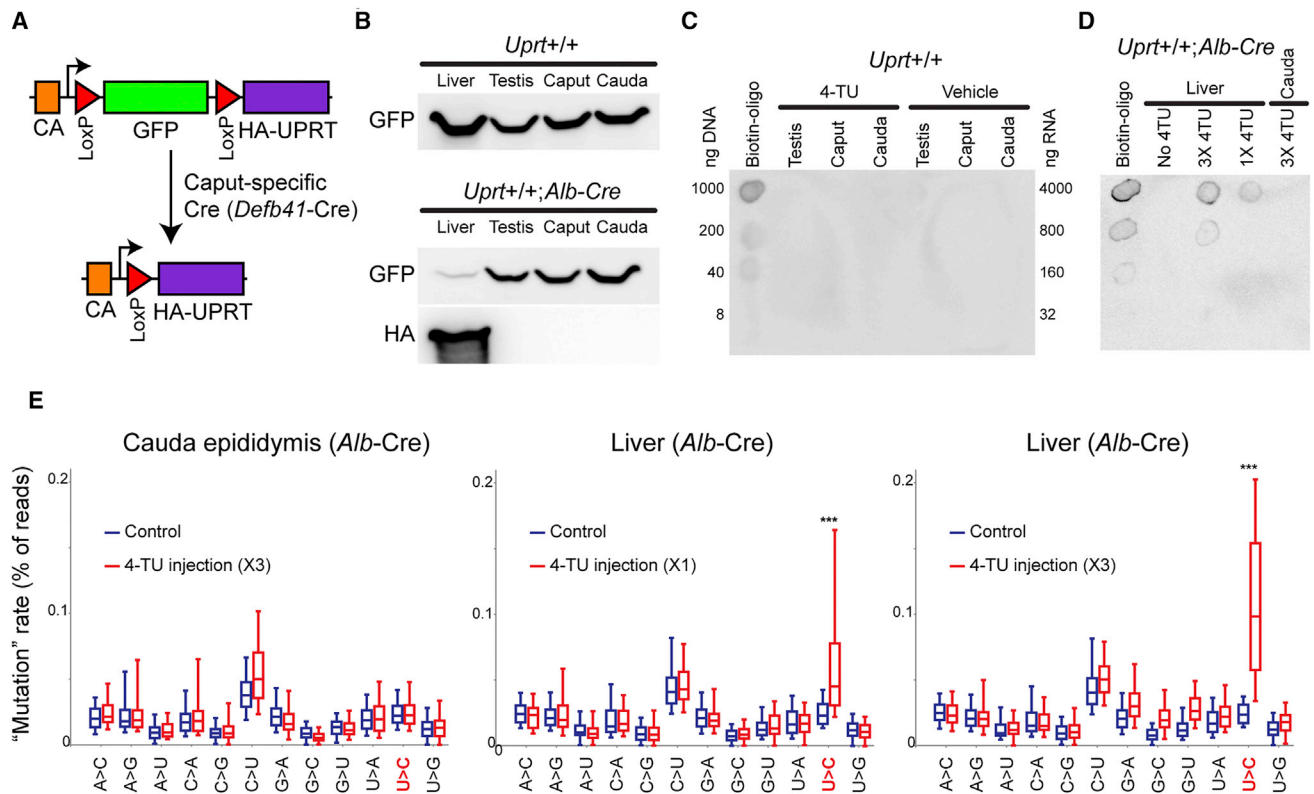


Figure 5. Tissue-Specific Labeling and Detection of Small RNAs in Intact Animals

(A) Schematic of the TU tracer locus. In the absence of Cre, GFP is expressed from a ubiquitous promoter, with no UPRT expression. Cre drives LoxP recombination, eliminating GFP and juxtaposing the promoter with HA-UPRT.

(B) Western blot showing GFP and HA-UPRT levels in livers and several reproductive tissues isolated from TU-tracer animals not expressing Cre (top) or expressing liver-specific *Albumin* promoter-driven Cre recombinase (bottom). In the absence of Cre, GFP is expressed from a ubiquitous promoter, with no UPRT expression. In mice expressing liver-specific Cre recombinase, HA-UPRT expression is confined to the liver, while the concomitant near-complete elimination of GFP underlines the relatively homogeneous cellular makeup of this tissue. See [Figure S4A](#) for uncropped western blot images.

(C) Dot blot for RNA isolated from TU-tracer animals not expressing Cre and injected with either 4-TU or vehicle alone. As shown, only positive control (Biotinylated DNA oligo) is detectable upon incubation with Streptavidin-HRP.

(D) Dot blot for RNA isolated from *Alb-Cre* X TU tracer mice injected with two different doses of 4-TU. Upon 4-TU injection, RNAs are specifically labeled, in a dose-dependent manner, in liver tissue and not in control tissue (cauda epididymis).

(E) SLAM-Seq analysis of 4-TU-labeled RNAs. TU tracer X *Alb-Cre* animals were either injected with 4-TU (400 mg/kg body weight) or with vehicle (solvent only) and were sacrificed 5–6 hr after the last injection for tissue harvest. Small RNAs were isolated from either cauda epididymis or from liver and subject to SLAM-Seq, and sequencing reads were mapped to microRNAs using an error-tolerant pipeline. Mismatches were identified for all reads mapping to a given microRNA, and boxplots (box: 25th/50th/75th percentile; whiskers: 10th/90th percentile) show the frequency of various mismatches for mock-injected and 4-TU-injected animals, as indicated.

Although tracking TU-labeled RNAs *in vivo* could, in principle, be accomplished by biotinylation of 4-TU ([Figures 5C and 5D](#)) and deep sequencing of avidin-purified RNAs, we note that even in an abundant tissue such as the liver only a very small fraction of RNA was 4-TU-labeled, and the abundance of any RNAs trafficked between cells would of course be far lower. Along with the fact that sperm overall have very low levels of total RNA, we anticipated extreme difficulty in the purification of rare biotinylated RNAs. We therefore turned instead to thiol(S)-linked alkylation for the metabolic sequencing of RNA (SLAM-Seq) ([Alberti et al., 2018](#); [Herzog et al., 2017](#)) for the characterization of 4-TU-labeled small RNAs. This method is based on chemically modifying the 4-thiouracil in RNA with iodoacetamide to generate a covalent adduct that causes nucleotide misincorporation during reverse transcription, with G misincorporation

opposite the modified U (seen as a U->C mutation in downstream deep sequencing) occurring most frequently. This method enables the quantitative analysis of 4-TU incorporation in any clonable population of small RNAs, sidestepping inevitable RNA losses during biotin purification. To characterize the signal-to-noise ratio for this method, we first applied SLAM-Seq to small RNAs purified from the liver of *Alb-Cre*-expressing mice. Background mutation rates in the cloning process were characterized using *Alb-Cre* mice that had not been injected with 4-TU, while analysis of cauda epididymis in these animals controlled for both cloning errors and for 4-TU incorporation into non-UPRT-expressing cells. As expected, we found that 4-TU incorporation caused a significant increase in U->C misincorporation events ([Figure 5E](#)). This required 4-TU injection, was dose dependent, and required the tissue-specific expression of

UPRT. Variation in the extent of U->C misincorporation for individual microRNAs reflects *in vivo* RNA synthesis and decay rates, as well as any effects of local sequence context on RT misincorporation. Together, these results demonstrate our ability to identify RNAs first synthesized in a given genetically defined cell type.

We therefore applied this system to track microRNAs synthesized in the caput epididymis, using the *Defb41* promoter (Björkgren et al., 2012) to drive Cre in the most proximal “initial segment” of the caput epididymis (Figure 6A). Mice carrying both the TU tracer cassette and *Defb41*-Cre exhibited the expected caput-specific expression of UPRT (Figures 6B and S4B). The injection of 4-TU into these animals resulted in caput-specific incorporation of 4-TU as assessed by biotinylation of total RNA (Figure S4C), and SLAM-Seq analysis of microRNAs purified from uninjected and TU-injected animals confirmed the expected TU-dependent increase in U->C mutation rates in caput epididymis RNAs, along with no change in U->C mutation rates in the testis (Figures 6C and 6D; Table S6).

Confident that we could reliably detect small RNAs synthesized in the caput epididymis, we finally turned to SLAM-Seq analysis of small RNAs purified from cauda epididymal sperm. Consistent with the hypothesis that cauda sperm carry microRNAs originally synthesized in the caput epididymis, SLAM-Seq of cauda sperm microRNAs revealed significantly greater 4-TU labeling than testes (Figures 6C and 6D; Figure S4D). Although this effect is quantitatively modest, it was significant in two biological replicates—Figure S4D shows the cumulative distribution plots for U->C mutations across all microRNAs for these samples. Taken together, these data conclusively demonstrate that at least a subset of small RNAs in mature sperm are originally synthesized in the caput epididymis and further support our hypothesis that small RNAs are trafficked from epididymis to sperm via epididymosomes.

DISCUSSION

Our data provide a detailed view of the biogenesis of the small RNA repertoire of maturing mammalian sperm. We characterized dynamics of small RNAs across sperm development, finding that multiple waves of small RNAs are synthesized or loaded into sperm over the course of testicular spermatogenesis and post-testicular maturation in the epididymis. Moreover, we show that caput epididymosomes can deliver small RNAs to testicular spermatozoa *in vitro* and use *in vivo* chemogenetic tracking in intact animals to definitively identify epididymis-derived RNAs in mature sperm. Together, our data reveal a surprising role for soma-to-germline trafficking in sculpting the sperm RNA payload.

An Improved Characterization of Sperm RNA Payload

Increasing interest in the functional roles for sperm RNAs in early development (see Conine et al., 2018 in this issue of *Developmental Cell*) has resulted in a number of studies reporting on the sperm RNA payload, with at times conflicting results. Here, we further refine our understanding of sperm small RNAs. Most notably, we find that a substantial additional population of 5' tRFs is revealed following PNK treatment to resolve cyclic 2'-3' phosphates. This is consistent with well-characterized roles

for RNase A family members such as Angiogenin (Fu et al., 2009; Yamasaki et al., 2009) and RNase T family members (Andersen and Collins, 2012; Lee and Collins, 2005; Thompson et al., 2008), in tRNA cleavage in various organisms. We note that although Angiogenin is not expressed at particularly high levels in the epididymis, several epididymis-specific paralogs of *Ang—Rnase 9–12*—are extremely highly expressed in this tissue, along with *Rnaset2a* (Castella et al., 2004; Johnston et al., 2005). These are therefore the likeliest nucleases responsible for the unusually high levels of tRNA cleavage observed in this tissue under unstressed conditions. Our data strongly suggest that RNaseA or T enzymes first cleave mature tRNAs at exposed loop regions, most notably the anticodon but in some cases also at the D or T loops, with exonuclease trimming or other degradation processes resulting in the slightly shorter 5' tRFs previously reported in multiple studies.

What happens to the 3' ends of cleaved tRNAs? Scrutiny of our small RNA datasets reveals low levels of reads (~10–100 ppm, compared to ~10–50,000 ppm for abundant 5' tRFs) mapping to the 3' ends of tRNAs, generally including the non-templated CCA found at the 3' ends of mature tRNAs. Ongoing studies suggest that 3' fragments resulting from tRNA cleavage are inherently challenging to clone, as we can robustly detect 3' tRNA cleavage products by northern blotting of epididymal RNAs (Figure S5). Although recent studies have documented enhanced full-length tRNA cloning following RNA demethylation with an engineered AlkB RNA demethylase (Cozen et al., 2015; Zheng et al., 2015), we have been unsuccessful thus far in enhancing 3' tRF capture using this enzyme (not shown), possibly owing to our inability to successfully generate deep sequencing libraries using the thermostable RT reported by Zheng et al. We anticipate that advances in cloning will enable a more quantitative capture of 3' tRFs from mature sperm RNA populations, which is a key goal for future studies, given the potential roles for 3' tRFs in LTR element control (Martinez et al., 2017; Schorn et al., 2017).

Small RNA Dynamics throughout Sperm Maturation

The analysis of small RNA repertoires of various purified sperm populations confirmed prior reports of a global loss of piRNAs and gain of tRFs that occurs over the course of post-testicular maturation and further defined a narrow anatomical window during which this transition occurs. In addition to this large-scale remodeling of the sperm small RNA payload, we also identified more subtle dynamic behaviors for a subset of RNAs. Most interestingly, a large group of microRNAs known to be expressed during spermatogenesis were abundant, as expected, in testicular sperm populations but were then surprisingly lost in caput epididymal sperm before recovering in abundance in cauda sperm (Figure 3). The majority of microRNAs exhibiting this behavior are encoded in genomic clusters, including the imprinted X-linked miR-880 cluster, the miR-17-92 “oncomiR” cluster, and many smaller clusters. Intriguingly, in the accompanying study (Conine et al., 2018), we find that embryos generated from caput sperm exhibit defects in pre-implantation gene regulation and that these gene regulatory defects seem to result from the transient loss of these clustered microRNAs in caput sperm.

Understanding the basis for this unusual behavior will be of great interest. The likeliest scenario is that these microRNAs

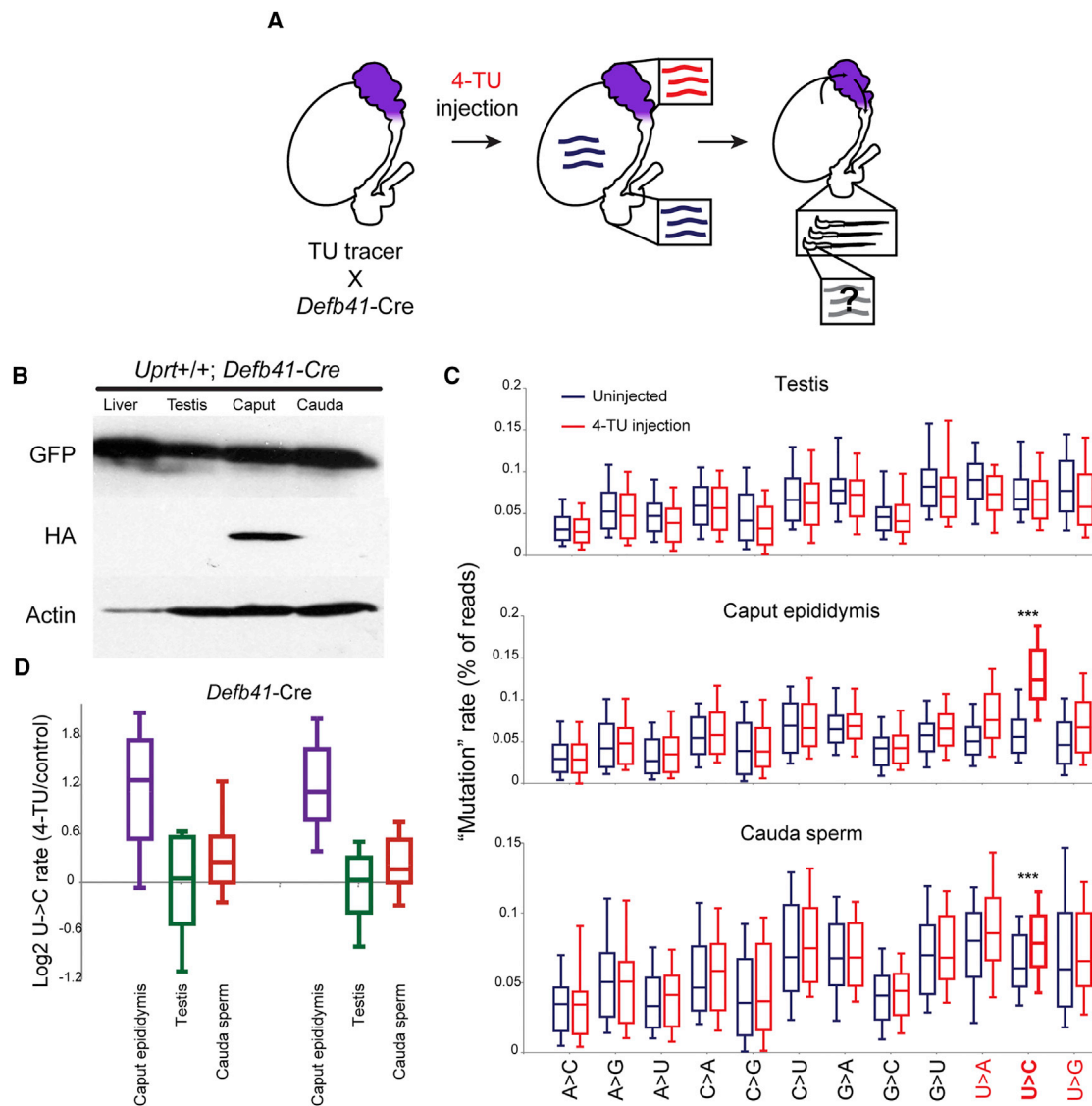


Figure 6. Chemogenetic Tracking of RNAs from Epididymis to Sperm

(A) Experimental design. UPRT is expressed specifically in the initial segment of the caput epididymis due to the expression of *Defb41-Cre*. Upon injection of 4-thiouracil (4-TU), RNAs synthesized in this tissue incorporate 4-TU. Animals are injected with 4-TU every 2 days for 9 days (5 injections), and 5 hr after injection on day 9, sperm are isolated from the cauda epididymis and assayed for 4-TU labeling of small RNAs.

(B) Western blots showing HA-UPRT expression specifically in the caput epididymis of *Defb41-Cre* X TU-tracer animals. Note that in contrast to the near-complete loss of GFP in *Alb-Cre* animals (Figure 5B), the continued expression of GFP in the caput epididymis is consistent with our expectation that only a limited subsection of the caput epididymis—the initial segment—expresses *Defb41*. See Figure S4B for uncropped western blot images.

(C) SLAM-Seq induces miscloning of uracil in a Cre- and 4-TU-dependent manner. *Defb41-Cre* X TU-tracer animals were either injected with 4-TU (every other day for 9 days) or sham-injected, and testis, caput epididymis, and cauda epididymal sperm were dissected. Small RNAs were purified and subject to SLAM-Seq. Reads were mapped to microRNAs using a mismatch-tolerant custom pipeline (STAR Methods) and nucleotide misreads were compiled for all microRNAs with at least 1,000 reads (boxes show median and 25th/75th percentiles, whiskers show 10th and 90th percentiles). 4-TU induces a misreading of uracils specifically in the caput epididymis, but not the testis, with U->C being the most common mutation observed ($p = 1.3e-42$, paired t test). Importantly, U->C mutations were also significantly ($p = 7.4e-7$, paired t test) elevated in a 4-TU-dependent manner in cauda sperm obtained from animals expressing Cre specifically in the caput epididymis epithelium (bottom panel).

(D) Log₂ ratio of U->C rates for 4-TU injected vs. uninjected animals, for all microRNAs with at least 1,000 reads for the indicated tissues. Boxplots show the distribution of log₂ fold change in U->C “mutation” rates for the three indicated tissues, with two separate replicates shown. The modest increase in U->C mutation in mature sperm reflects multiple factors: (1) the signal-to-noise in caput epididymis is already modest (2-fold); (2) cauda sperm carry a wide range of unlabeled RNAs originating in the testis and other parts of the epididymis; and (3) sperm in the cauda epididymis can survive for longer than the time frame of this experiment and so will include a population of unlabeled sperm that passed through the caput epididymis prior to 4-TU injections.

(along with the bulk of piRNAs) are degraded, or ejected in the cytoplasmic droplet (Sprando and Russell, 1987), upon epididymal entry. Clustered microRNAs would then be either trafficked from the epididymis to transiting sperm in epididymosomes or, less likely, generated *in situ* via processing of precursor transcripts. An extreme version of this model is that entry into the epididymis is accompanied by a global purge of *all* small RNAs including all microRNAs, with the microRNAs that seem to maintain abundance in caput epididymis (such as various let-7 family members) simply being those that are replenished earlier than the clustered microRNAs that are gained more distally. Whatever the mechanism for this process, the reason for the strong caput/cauda gradients in the expression and trafficking of various small RNAs remains unclear and will be the subject of future studies.

Soma-to-Germline RNA Trafficking in the Epididymis

How do transcriptionally inactive sperm gain new small RNAs during epididymal transit? Multiple lines of evidence support the hypothesis that small RNAs synthesized in the epididymis epithelium are trafficked to maturing sperm in small extracellular vesicles, collectively known as epididymosomes: (1) Small RNAs that are gained as sperm enter the epididymis, such as tRFs, are highly abundant in the epididymis epithelium. (2) More locally, gradients in small RNA expression between the proximal and distal epididymis are manifest in sperm transiting the relevant region (as in, e.g., the ~10-fold difference in tRF-Val-CAC between caput and cauda epididymis, sperm, and epididymosomes). (3) Using the TU tracer system, we show here that microRNAs first synthesized in the caput epididymis make their way to maturing sperm, thus demonstrating that the soma-to-germline transfer of small RNAs occurs in intact animals. (4) The likely mechanism for this transfer is RNA trafficking in epididymosomes, as purified epididymosomes carry a very similar RNA payload to that gained by sperm during epididymal transit. (5) Epididymosomes can deliver small RNAs to sperm *in vitro*.

Our data thus identify a role for soma-to-germline trafficking in shaping the sperm RNA repertoire in mammalian sperm. This unites mammalian spermatogenesis with gametogenesis in a number of other species where RNAs produced in somatic support cells have been suggested or shown to be subsequently transferred into developing germ cells (Bourc'his and Voinnet, 2010). Previously described or proposed examples of such soma-to-germline communication include the following: (1) communication between the somatic macronucleus and the germline micronucleus in ciliates such as *Tetrahymena* (Mochizuki et al., 2002) and *Oxytricha* (Fang et al., 2012), (2) piRNA communication from somatic follicle cells to the germline during *Drosophila* oogenesis (Ghildiyal and Zamore, 2009; Malone et al., 2009), and (3) release of transposon repression in vegetative nuclei in *Arabidopsis* pollen leading to the generation of anti-transposon siRNAs, which are transported into the sperm nuclei (Martínez et al., 2016; Slotkin et al., 2009).

Intriguingly, the process detailed here is quite distinct from most prior examples of soma-to-germline communication, as the proposed trafficking process involves a vesicle intermediate rather than direct cytoplasmic connections (Mahajan-Miklos and Cooley, 1994; McCue et al., 2011), and the RNAs being shipped are primarily microRNAs and tRFs as opposed to repeat element-derived piRNAs/siRNAs. Importantly, although a multi-

tude of cell types secrete RNAs into extracellular vesicles in mammals (Tkach and Théry, 2016), there is as yet no evidence that circulating vesicles have direct access to the germline, which is protected by the blood-testis barrier—for example, we find no evidence in the *Alb-Cre* X TU-tracer experiments for liver-to-germline communication. Thus, the epididymis, along with somatic cells of the testis such as Sertoli cells, occupies a privileged position in this regard.

Epigenetic Remodeling during Gametogenesis

Many potentially heritable “epigenetic marks” in the germline are known to be erased during key stages of development, as, for example, cytosine methylation patterns undergo two major waves of erasure and re-establishment during the mammalian life cycle (Feng et al., 2010)—once in primordial germ cells and again shortly after fertilization. Our findings reveal novel epigenetic reprogramming events that occur during mammalian spermatogenesis, as we document a major transition from a piRNA-dominated stage of testicular spermatogenesis to the ultimately tRF-dominated payload of epididymal sperm, as well as a transient loss of clustered microRNAs that occurs in the caput epididymis.

The mechanism by which this epigenetic remodeling occurs is of significant interest, given the mounting evidence that environmental signaling may be able to modulate specific epigenetic marks in germ cells and thereby potentially affect the phenotype in future generations (Chen et al., 2016b; Lane et al., 2014; Rando, 2012). Though it is well appreciated that, say, an organism's dietary conditions can influence the epigenome in somatic cells (Sharma and Rando, 2017), it has not been clear how this information is communicated to the developing gametes and thus to offspring. The origin of sperm small RNAs in the epididymis provides a focus for future studies on the mechanism by which environmental conditions might influence the sperm epigenome. Understanding the molecular basis underlying sorting and packaging of small RNAs into epididymosomes will also be of great interest (Gutiérrez-Vázquez et al., 2013; Koppers-Lalic et al., 2014), as it will not only uncover a basic mechanism of communication between the somatic cells of epididymis and the maturing gametes but will also shed light on how environmental information is signaled to sperm.

STAR★METHODS

Detailed methods are provided in the online version of this paper and include the following:

- KEY RESOURCES TABLE
- CONTACT FOR REAGENT AND RESOURCE SHARING
- EXPERIMENTAL MODEL AND SUBJECT DETAILS
 - Mice
- METHOD DETAILS
 - Tissue and Sperm Isolation
 - Sperm Washing
 - Separation of Sperm Head and Tail
 - Epididymosome Isolation
 - Testicular Spermatozoa and Caput Epididymosome Fusion
 - PNK Treatment

- Small RNA Deep Sequencing
- TaqMan Assays
- Generation of Mice Expressing Tissue-Specific UPRT
- 4-Thiouracil (4-TU) Treatment
- Northern and Dot Blot Analysis
- Western Blot
- SLAM-Seq
- **QUANTITATION AND STATISTICAL ANALYSIS**
- **DATA AND SOFTWARE AVAILABILITY**

SUPPLEMENTAL INFORMATION

Supplemental information includes five figures and six tables and can be found with this article online at <https://doi.org/10.1016/j.devcel.2018.06.023>.

ACKNOWLEDGMENTS

We thank members of the Rando lab for their critical reading of the manuscript and helpful comments. We thank P. Sipilä for the generous gift of the *Defb41*: Cre mouse strain. This work was supported by NIH grants R01HD080224 and DP1ES025458 (O.J.R.) and by the Austrian Academy of Sciences and the European Research Council ERC-StG-338252 (SLA). U.S. is a Charles H. Hood postdoctoral fellow. C.C.C. is a Helen Hay Whitney Foundation postdoctoral fellow.

AUTHOR CONTRIBUTIONS

The majority of the experiments were designed by U.S. and O.J.R. U.S. carried out RNA characterizations in epididymosomes and various sperm populations and carried out epididymosome fusion experiments. S.K., F.S., and C.C.C. carried out analyses of sperm wash conditions and RNA treatments; F.S. purified testicular sperm populations; F.S. and U.S. carried out TU tracer experiments; and SLAM-Seq was performed and analyzed by B.R., V.A.H., and S.L.S. U.S. and O.J.R. carried out most data analysis and wrote the manuscript, which was reviewed and edited by all authors.

DECLARATION OF INTERESTS

The authors declare no competing interests.

Received: August 3, 2017

Revised: May 11, 2018

Accepted: June 26, 2018

Published: July 26, 2018

REFERENCES

Alberti, C., Manzenreither, R.A., Sowemimo, I., Burkard, T.R., Wang, J., Mahofsky, K., Ameres, S.L., and Cochella, L. (2018). Cell-type specific sequencing of microRNAs from complex animal tissues. *Nat. Methods* *15*, 283–289.

Andersen, K.L., and Collins, K. (2012). Several RNase T2 enzymes function in induced tRNA and rRNA turnover in the ciliate *Tetrahymena*. *Mol. Biol. Cell* *23*, 36–44.

Anderson, P., and Ivanov, P. (2014). tRNA fragments in human health and disease. *FEBS Lett.* *588*, 4297–4304.

Aravin, A., Gaidatzis, D., Pfeffer, S., Lagos-Quintana, M., Landgraf, P., Iovino, N., Morris, P., Brownstein, M.J., Kuramochi-Miyagawa, S., Nakano, T., et al. (2006). A novel class of small RNAs bind to MILI protein in mouse testes. *Nature* *442*, 203–207.

Aravin, A.A., Sachidanandam, R., Girard, A., Fejes-Toth, K., and Hannon, G.J. (2007). Developmentally regulated piRNA clusters implicate MILI in transposon control. *Science* *316*, 744–747.

Arteaga-Vazquez, M.A., and Chandler, V.L. (2010). Paramutation in maize: RNA mediated trans-generational gene silencing. *Curr. Opin. Genet. Dev.* *20*, 156–163.

Batista, P.J., Ruby, J.G., Claycomb, J.M., Chiang, R., Fahlgren, N., Kasschau, K.D., Chaves, D.A., Gu, W., Vasale, J.J., Duan, S., et al. (2008). PRG-1 and 21U-RNAs interact to form the piRNA complex required for fertility in *C. elegans*. *Mol. Cell* *31*, 67–78.

Belleannée, C., Calvo, É., Caballero, J., and Sullivan, R. (2013). Epididymosomes convey different repertoires of microRNAs throughout the bovine epididymis. *Biol. Reprod.* *89*, 30.

Björkgren, I., Saastamoinen, L., Krutskikh, A., Huhtaniemi, I., Poutanen, M., and Sipilä, P. (2012). Dicer1 ablation in the mouse epididymis causes dedifferentiation of the epithelium and imbalance in sex steroid signaling. *PLOS ONE* *7*, e38457.

Bourc'his, D., and Voinnet, O. (2010). A small-RNA perspective on gametogenesis, fertilization, and early zygotic development. *Science* *330*, 617–622.

Brennecke, J., Aravin, A.A., Stark, A., Dus, M., Kellis, M., Sachidanandam, R., and Hannon, G.J. (2007). Discrete small RNA-generating loci as master regulators of transposon activity in *Drosophila*. *Cell* *128*, 1089–1103.

Brennecke, J., Malone, C.D., Aravin, A.A., Sachidanandam, R., Stark, A., and Hannon, G.J. (2008). An epigenetic role for maternally inherited piRNAs in transposon silencing. *Science* *322*, 1387–1392.

Castella, S., Benedetti, H., de Llorens, R., Dacheux, J.L., and Dacheux, F. (2004). Train A, an RNase A-like protein without RNase activity, is secreted and reabsorbed by the same epididymal cells under testicular control. *Biol. Reprod.* *71*, 1677–1687.

Chen, Q., Yan, M., Cao, Z., Li, X., Zhang, Y., Shi, J., Feng, G.H., Peng, H., Zhang, X., Zhang, Y., et al. (2016a). Sperm tsRNAs contribute to intergenerational inheritance of an acquired metabolic disorder. *Science* *351*, 397–400.

Chen, Q., Yan, W., and Duan, E. (2016b). Epigenetic inheritance of acquired traits through sperm RNAs and sperm RNA modifications. *Nat. Rev. Genet.* *17*, 733–743.

Conine, C.C., Sun, F., Song, L., Rivera-Pérez, J.A., and Rando, O.J. (2018). Small RNAs gained during epididymal transit of sperm are essential for embryonic development in mice. *Dev. Cell* *46*. Published online July 26, 2018. <https://doi.org/10.1016/j.devcel.2018.06.024>.

Couvillion, M.T., Sachidanandam, R., and Collins, K. (2010). A growth-essential *Tetrahymena* Piwi protein carries tRNA fragment cargo. *Genes. Dev.* *24*, 2742–2747.

Cozen, A.E., Quartley, E., Holmes, A.D., Hrabeta-Robinson, E., Phizicky, E.M., and Lowe, T.M. (2015). ARM-seq: AlkB-facilitated RNA methylation sequencing reveals a complex landscape of modified tRNA fragments. *Nat. Methods* *12*, 879–884.

de Castro Barbosa, T., Ingerslev, L.R., Alm, P.S., Versteyhe, S., Massart, J., Rasmussen, M., Donkin, I., Sjögren, R., Mudry, J.M., Vetterli, L., et al. (2016). High-fat diet reprograms the epigenome of rat spermatozoa and transgenerationally affects metabolism of the offspring. *Mol. Metab.* *5*, 184–197.

de Mateo, S., and Sassone-Corsi, P. (2014). Regulation of spermatogenesis by small non-coding RNAs: role of the germ granule. *Semin. Cell. Dev. Biol.* *29*, 84–92.

de Vanssay, A., Bougé, A.L., Boivin, A., Hermant, C., Teyssier, L., Delmarre, V., Antoniewski, C., and Ronsseray, S. (2012). Paramutation in *Drosophila* linked to emergence of a piRNA-producing locus. *Nature* *490*, 112–115.

Emara, M.M., Ivanov, P., Hickman, T., Dawra, N., Tisdale, S., Kedersha, N., Hu, G.F., and Anderson, P. (2010). Angiogenin-induced tRNA-derived stress-induced RNAs promote stress-induced stress granule assembly. *J. Biol. Chem.* *285*, 10959–10968.

Fang, W., Wang, X., Bracht, J.R., Nowacki, M., and Landweber, L.F. (2012). Piwi-interacting RNAs protect DNA against loss during *Oxytricha* genome rearrangement. *Cell* *151*, 1243–1255.

Feng, S., Jacobsen, S.E., and Reik, W. (2010). Epigenetic reprogramming in plant and animal development. *Science* *330*, 622–627.

Fire, A., Xu, S., Montgomery, M.K., Kostas, S.A., Driver, S.E., and Mello, C.C. (1998). Potent and specific genetic interference by double-stranded RNA in *Caenorhabditis elegans*. *Nature* *391*, 806–811.

- Fu, H., Feng, J., Liu, Q., Sun, F., Tie, Y., Zhu, J., Xing, R., Sun, Z., and Zheng, X. (2009). Stress induces tRNA cleavage by angiogenin in mammalian cells. *FEBS Lett* 583, 437–442.
- Gapp, K., Jawaid, A., Sarkies, P., Bohacek, J., Pelczar, P., Prados, J., Farinelli, L., Miska, E., and Mansuy, I.M. (2014). Implication of sperm RNAs in transgenerational inheritance of the effects of early trauma in mice. *Nat. Neurosci.* 17, 667–669.
- García-López, J., Hourcade, Jde D., Alonso, L., Cárdenas, D.B., and Del Mazo, J. (2014). Global characterization and target identification of piRNAs and endo-siRNAs in mouse gametes and zygotes. *Biochim. Biophys. Acta* 1839, 463–475.
- Gay, L., Miller, M.R., Ventura, P.B., Devasthali, V., Vue, Z., Thompson, H.L., Temple, S., Zong, H., Cleary, M.D., Stankunas, K., et al. (2013). Mouse TU tagging: a chemical/genetic intersectional method for purifying cell type-specific nascent RNA. *Genes. Dev.* 27, 98–115.
- Ghildiyal, M., and Zamore, P.D. (2009). Small silencing RNAs: an expanding universe. *Nat. Rev. Genet.* 10, 94–108.
- Gutiérrez-Vázquez, C., Villarroya-Beltri, C., Mittelbrunn, M., and Sánchez-Madrid, F. (2013). Transfer of extracellular vesicles during immune cell-cell interactions. *Immunol. Rev.* 251, 125–142.
- Hamilton, A.J., and Baulcombe, D.C. (1999). A species of small antisense RNA in posttranscriptional gene silencing in plants. *Science* 286, 950–952.
- Herzog, V.A., Reichholf, B., Neumann, T., Rescheneder, P., Bhat, P., Burkard, T.R., Wlotzka, W., von Haeseler, A., Zuber, J., and Ameres, S.L. (2017). Thiol-linked alkylation of RNA to assess expression dynamics. *Nat. Methods* 14, 1198–1204.
- Jayaprakash, A.D., Jhabdo, O., Brown, B.D., and Sachidanandam, R. (2011). Identification and remediation of biases in the activity of RNA ligases in small-RNA deep sequencing. *Nucleic Acids Res.* 39, e141.
- Johnston, D.S., Jelinsky, S.A., Bang, H.J., DiCandeloro, P., Wilson, E., Kopf, G.S., and Turner, T.T. (2005). The mouse epididymal transcriptome: transcriptional profiling of segmental gene expression in the epididymis. *Biol. Reprod.* 73, 404–413.
- Kawano, M., Kawaji, H., Grandjean, V., Kiani, J., and Rassoulzadegan, M. (2012). Novel small noncoding RNAs in mouse spermatozoa, zygotes and early embryos. *PLOS ONE* 7, e44542.
- Koppers-Lalic, D., Hackenberg, M., Bijnsdorp, I.V., van Eijndhoven, M.A.J., Sadek, P., Sie, D., Zini, N., Middeldorp, J.M., Ylstra, B., de Menezes, R.X., et al. (2014). Nontemplated nucleotide additions distinguish the small RNA composition in cells from exosomes. *Cell. Rep.* 8, 1649–1658.
- Kozomara, A., and Griffiths-Jones, S. (2014). miRBase: annotating high confidence microRNAs using deep sequencing data. *Nucleic Acids Res.* 42, D68–D73.
- Krapf, D., Ruan, Y.C., Wertheimer, E.V., Battistone, M.A., Pawlak, J.B., Sanjay, A., Pilder, S.H., Cuasnicu, P., Breton, S., and Visconti, P.E. (2012). cSrc is necessary for epididymal development and is incorporated into sperm during epididymal transit. *Dev. Biol.* 369, 43–53.
- Kuramochi-Miyagawa, S., Kimura, T., Ijiri, T.W., Isobe, T., Asada, N., Fujita, Y., Ikawa, M., Iwai, N., Okabe, M., Deng, W., et al. (2004). Mili, a mammalian member of piwi family gene, is essential for spermatogenesis. *Development* 131, 839–849.
- Lane, M., Robker, R.L., and Robertson, S.A. (2014). Parenting from before conception. *Science* 345, 756–760.
- Langmead, B., Trapnell, C., Pop, M., and Salzberg, S.L. (2009). Ultrafast and memory-efficient alignment of short DNA sequences to the human genome. *Genome Biol.* 10, R25.
- Lee, S.R., and Collins, K. (2005). Starvation-induced cleavage of the tRNA anticodon loop in *Tetrahymena thermophila*. *J. Biol. Chem.* 280, 42744–42749.
- Lee, Y.S., Shibata, Y., Malhotra, A., and Dutta, A. (2009). A novel class of small RNAs: tRNA-derived RNA fragments (tRFs). *Genes. Dev.* 23, 2639–2649.
- Li, X.Z., Roy, C.K., Dong, X., Bolcun-Filas, E., Wang, J., Han, B.W., Xu, J., Moore, M.J., Schimenti, J.C., Weng, Z., et al. (2013). An ancient transcription factor initiates the burst of piRNA production during early meiosis in mouse testes. *Mol. Cell* 50, 67–81.
- Malahan-Miklos, S., and Cooley, L. (1994). Intercellular cytoplasm transport during *Drosophila* oogenesis. *Dev. Biol.* 165, 336–351.
- Malone, C.D., Brennecke, J., Dus, M., Stark, A., McCombie, W.R., Sachidanandam, R., and Hannon, G.J. (2009). Specialized piRNA pathways act in germline and somatic tissues of the *Drosophila* ovary. *Cell* 137, 522–535.
- Martinez, G., Choudury, S.G., and Slotkin, R.K. (2017). tRNA-derived small RNAs target transposable element transcripts. *Nucleic Acids Res.* 45, 5142–5152.
- Martínez, G., Panda, K., Köhler, C., and Slotkin, R.K. (2016). Silencing in sperm cells is directed by RNA movement from the surrounding nurse cell. *Nat. Plants* 2, 16030.
- McCue, A.D., Cresti, M., Feijó, J.A., and Slotkin, R.K. (2011). Cytoplasmic connection of sperm cells to the pollen vegetative cell nucleus: potential roles of the male germ unit revisited. *J. Exp. Bot.* 62, 1621–1631.
- Meikar, O., Da Ros, M., Korhonen, H., and Kotaja, N. (2011). Chromatoid body and small RNAs in male germ cells. *Reproduction* 142, 195–209.
- Mochizuki, K., Fine, N.A., Fujisawa, T., and Gorovsky, M.A. (2002). Analysis of a piwi-related gene implicates small RNAs in genome rearrangement in tetrahymena. *Cell* 110, 689–699.
- Nixon, B., Stanger, S.J., Mihalas, B.P., Reilly, J.N., Anderson, A.L., Tyagi, S., Holt, J.E., and McLaughlin, E.A. (2015). The microRNA signature of mouse spermatozoa is substantially modified during epididymal maturation. *Biol. Reprod.* 93, 91.
- Peng, H., Shi, J., Zhang, Y., Zhang, H., Liao, S., Li, W., Lei, L., Han, C., Ning, L., Cao, Y., et al. (2012). A novel class of tRNA-derived small RNAs extremely enriched in mature mouse sperm. *Cell. Res.* 22, 1609–1612.
- Rädle, B., Rutkowski, A.J., Ruzsics, Z., Friedel, C.C., Koszinowski, U.H., and Dölken, L. (2013). Metabolic labeling of newly transcribed RNA for high resolution gene expression profiling of RNA synthesis, processing and decay in cell culture. *J. Vis. Exp.* 78, e50195.
- Rando, O.J. (2012). Daddy issues: paternal effects on phenotype. *Cell* 151, 702–708.
- Rassoulzadegan, M., Grandjean, V., Gounon, P., Vincent, S., Gillot, I., and Cuzin, F. (2006). RNA-mediated non-Mendelian inheritance of an epigenetic change in the mouse. *Nature* 441, 469–474.
- Reilly, J.N., McLaughlin, E.A., Stanger, S.J., Anderson, A.L., Hutcheon, K., Church, K., Mihalas, B.P., Tyagi, S., Holt, J.E., Eamens, A.L., et al. (2016). Characterisation of mouse epididymosomes reveals a complex profile of microRNAs and a potential mechanism for modification of the sperm epigenome. *Sci. Rep.* 6, 31794.
- Rodgers, A.B., Morgan, C.P., Leu, N.A., and Bale, T.L. (2015). Transgenerational epigenetic programming via sperm microRNA recapitulates effects of paternal stress. *Proc. Natl. Acad. Sci. USA* 112, 13699–13704.
- Rompala, G.R., Mounier, A., Wolfe, C.M., Lin, Q., Lefterov, I., and Homanics, G.E. (2018). Heavy chronic intermittent ethanol exposure alters small noncoding RNAs in mouse sperm and epididymosomes. *Front. Genet.* 9, 32.
- Schorn, A.J., Gutbrod, M.J., LeBlanc, C., and Martienssen, R. (2017). LTR-retrotransposon control by tRNA-derived small RNAs. *Cell* 170, 61–71.e11.
- Schuster, A., Tang, C., Xie, Y., Ortogero, N., Yuan, S., and Yan, W. (2016). SpermBase: a database for sperm-borne RNA contents. *Biol. Reprod.* 95, 99.
- Sharma, U., Conine, C.C., Shea, J.M., Boskovic, A., Derr, A.G., Bing, X.Y., Belleanne, C., Kucukural, A., Serra, R.W., Sun, F., et al. (2016). Biogenesis and function of tRNA fragments during sperm maturation and fertilization in mammals. *Science* 351, 391–396.
- Sharma, U., and Rando, O.J. (2017). Metabolic inputs into the epigenome. *Cell. Metab.* 25, 544–558.
- Shirayama, M., Seth, M., Lee, H.C., Gu, W., Ishidate, T., Conte, D., Jr., and Mello, C.C. (2012). piRNAs initiate an epigenetic memory of nonself RNA in the *C. elegans* germline. *Cell* 150, 65–77.
- Slotkin, R.K., Vaughn, M., Borges, F., Tanurdzić, M., Becker, J.D., Feijó, J.A., and Martienssen, R.A. (2009). Epigenetic reprogramming and small RNA silencing of transposable elements in pollen. *Cell* 136, 461–472.

- Sobala, A., and Hutvagner, G. (2011). Transfer RNA-derived fragments: origins, processing, and functions. *Wiley Interdiscip. Rev. RNA* 2, 853–862.
- Sprando, R.L., and Russell, L.D. (1987). Comparative study of cytoplasmic elimination in spermatids of selected mammalian species. *Am. J. Anat.* 178, 72–80.
- Sullivan, R., Frenette, G., and Girouard, J. (2007). Epididymosomes are involved in the acquisition of new sperm proteins during epididymal transit. *Asian J. Androl.* 9, 483–491.
- Sullivan, R., and Saez, F. (2013). Epididymosomes, prostasomes, and liposomes: their roles in mammalian male reproductive physiology. *Reproduction* 146, R21–R35.
- Thompson, D.M., Lu, C., Green, P.J., and Parker, R. (2008). tRNA cleavage is a conserved response to oxidative stress in eukaryotes. *RNA* 14, 2095–2103.
- Tkach, M., and Théry, C. (2016). Communication by extracellular vesicles: where we are and where we need to go. *Cell* 164, 1226–1232.
- Vagin, V.V., Sigova, A., Li, C., Seitz, H., Gvozdev, V., and Zamore, P.D. (2006). A distinct small RNA pathway silences selfish genetic elements in the germline. *Science* 313, 320–324.
- Volpe, T.A., Kidner, C., Hall, I.M., Teng, G., Grewal, S.I., and Martienssen, R.A. (2002). Regulation of heterochromatic silencing and histone H3 lysine-9 methylation by RNAi. *Science* 297, 1833–1837.
- Yamasaki, S., Ivanov, P., Hu, G.F., and Anderson, P. (2009). Angiogenin cleaves tRNA and promotes stress-induced translational repression. *J. Cell. Biol.* 185, 35–42.
- Yang, A., Ha, S., Ahn, J., Kim, R., Kim, S., Lee, Y., Kim, J., Soll, D., Lee, H.Y., and Park, H.S. (2016). A chemical biology route to site-specific authentic protein modifications. *Science* 354, 623–626.
- Zheng, G., Qin, Y., Clark, W.C., Dai, Q., Yi, C., He, C., Lambowitz, A.M., and Pan, T. (2015). Efficient and quantitative high-throughput tRNA sequencing. *Nat. Methods* 12, 835–837.
- Zilberman, D., Cao, X., and Jacobsen, S.E. (2003). ARGONAUTE4 control of locus-specific siRNA accumulation and DNA and histone methylation. *Science* 299, 716–719.

STAR★METHODS

KEY RESOURCES TABLE

REAGENT or RESOURCE	SOURCE	IDENTIFIER
Antibodies		
GFP tag polyclonal antibody	Invitrogen	cat# A-11122; RRID: AB_221569
HA tag polyclonal antibody (SG77)	Thermo Fisher Scientific	cat# 71-5500; RRID: AB_2533988
Beta actin polyclonal antibody	Thermo Fisher Scientific	cat# PA1-183; RRID: AB_2608409
Anti-mouse IgG HRP-linked	Cell Signaling	cat# 7076S; RRID: AB_330924
Anti-rabbit IgG HRP-linked	Cell Signaling	cat# 7074S; RRID: AB_2099233
Chemicals, Peptides, and Recombinant Proteins		
Percoll, pH 8.5-9.5 (20 °C)	Sigma	cat# P1644
4-Thiouracil	Cayman chemical	cat#16952
T4 Polynucleotide Kinase (PNK)	NEB	cat# M0201
Critical Commercial Assays		
TruSeq small RNA library prep kit	Illumina	cat# RS-200-0012
NextSeq 500/550 High Output v2 kit (75 cycles)	Illumina	cat# FC-404-2005
SuperScript II	Invitrogen	cat# 18064-014
T4 RNA Ligase 2, Deletion Mutant	Epicenter	cat# LR2D1132K
TaqMan microRNA assays	Life Technologies	cat#4427975
TaqMan custom small RNA assays	Life Technologies	cat#4398987
TaqMan microRNA Reverse transcription kit	Life Technologies	cat#4366596
Deposited Data		
Raw and analyzed data	This paper	GEO: GSE112990
Experimental Models: Organisms/Strains		
Mouse: FVB/NJ (wild type)	The Jackson Laboratory	Jax001800; RRID:IMSR_JAX:001800
Mouse: <i>Defb41</i> iCre KI (TUKO 10) (<i>Defb41</i> -Cre)	Laboratory of Dr. Petra Sipilä	Bjorkgren et al.; 2012
Mouse: B6(D2)-Tg(CAG-GFP,-Uprt)985Cdoe/J (CAGFPstopUPRT mice)	The Jackson Laboratory	Jax021469; RRID:IMSR_JAX:021469
Mouse: B6.Cg-Speer6-ps1 ^{Tg(Alb-cre)21Mgn} /J (<i>Albumin</i> -Cre)	The Jackson Laboratory	Jax003574; RRID:IMSR_JAX:003574
Oligonucleotides		
Genotyping CAGFPstopUPRT mice mutant allele primers 5'-ATT CCA AGA TCT GTG GCG TC-3' and 5'-CTT CTC GTA GAT CAG CTT AGG C-3' for mutant allele	This study	N/A
Genotyping CAGFPstopUPRT mice wildtype allele primers 5'-CAC GTG GGC TCC AGC ATT-3' and 5'-TCA CCA GTC ATT TCT GCC TTT G-3' for wildtype allele	This study	N/A
Genotyping CAGFPstopUPRT mice wildtype allele probe 5'-/Cy5/CCA ATG GTC GGG CAC TGC TCA A/Black Hole Quencher 2/-3' for wildtype allele	This study	N/A
Genotyping CAGFPstopUPRT mice mutant allele probe 5'-/6-FAM/CCG CAT CGG GAA AAT CCT CAT CCA/Black Hole Quencher 2/-3'	This study	N/A
Genotyping Albumin-cre mice 5'-TTG GCC CCT TAC CAT AAC TG-3' for both wildtype and mutant allele	This study	N/A
Genotyping Albumin-cre mice 5'-TGC AAA CAT CAC ATG CAC AC-3' for wildtype allele	This study	N/A
Genotyping Albumin-cre mice 5'-GAA GCA GAA GCT TAG GAA GAT GG-3' for mutant allele	This study	N/A

(Continued on next page)

Continued

REAGENT or RESOURCE	SOURCE	IDENTIFIER
Primers for Defb41-cre mice trasgene: 5'-AGA TGC CAG GAC ATC AGG AAC CTG-3' and 5'-ATC AGC CAC ACC AGA CAC AGA GAT C-3'	This study	N/A
Primers for Defb41-cre mice internal positive control 5'-CTA GGC CAC AGA ATT GAA AGA TCT-3' and 5'-GTA GGT GGA AAT TCT AGC ATC ATC C-3'	This study	N/A
Northern blot analysis probe 3'tRF GlyGCC 5'TGCATTGG CCGGGAACCGAACCCGGGCTCCCGCG 3'	This study	N/A
Northern blot analysis probe 3'tRF Val CAC 5'TGTTTCCGCC CGGTTTCGAACCCGGGACCTTTTCGCG 3'	This study	N/A
Software and Algorithms		
SeqMapping	Umass Biocore	N/A
RSEM	Umass Biocore	N/A
Bowtie v.1.2	Langmead, et al. (2009)	http://bowtie-bio.sourceforge.net/index.shtml
mirbase v.21	Kozomara and Griffiths-Jones, (2014)	http://www.mirbase.org/

CONTACT FOR REAGENT AND RESOURCE SHARING

Further information and requests for resources and reagents should be directed to and will be fulfilled by the Lead Contact, Oliver J. Rando (oliver.rando@umassmed.edu).

EXPERIMENTAL MODEL AND SUBJECT DETAILS

Mice

All animal care and use procedures were in accordance with guidelines of University of Massachusetts Medical School Institutional Animal Care and Use Committee. Mice were group housed (maximum of 5 per cage) with a 12-hour light-dark cycle (lights off at 7 pm) and free access to food and water *ad libitum*. Mice were weaned from mothers at 21 days of age. All animals used for experiments were 8-12 weeks old and fed either control diet (Bioserv AIN-93g) or normal chow diet (TU-tracer experiments).

Wild type FVB/NJ mice obtained from Jackson Laboratory were used for all experiments other than TU-tracer experiments (Figures 5 and 6, Figure S4). For our breeding colonies, six week old FVB/NJ mice were purchased from Jackson Laboratory, and 24 hours after arrival at UMass Animal Facility mice were moved from chow to control diet (Bioserv AIN-93g). After being on the control diet for 2 weeks, mice were mated and the offspring were weaned on to control diet. The first three litters generated from the breeding pair were used for sperm and tissue isolations.

For TU-tracer experiments, B6(D2)-Tg(CAG-GFP,-Uprt)985Cdoe (CAGFPstopUPRT mice) and *Albumin-cre* (B6.Cg-Speer6-ps1^{Tg(Alb-cre)21Mgn/J}) mice were purchased from Jackson Laboratory. *Defb41* iCre KI (TUKO 10) mouse embryos were a gift from Dr. Petra Sipilä, Univeristy of Turku Finland. *Defb41* iCre KI (TUKO 10) mouse line was regenerated at the Mouse Facility of UMass Medical School.

METHOD DETAILS

Tissue and Sperm Isolation

Testes, epididymis, caput sperm, cauda sperm, spermatocytes and round spermatids were isolated as described previously (Sharma et al., 2016). Briefly, testes were dissected from 10-12 week mice, directly frozen in liquid nitrogen and stored at -80 °C until RNA extraction. Cauda and Caput epididymis were dissected from mice and placed in Whitten's Media (100 mM NaCl, 4.7 mM KCl, 1.2 mM KH₂PO₄, 1.2 mM MgSO₄, 5.5 mM Glucose, 1 mM Pyruvic acid, 4.8 mM Lactic acid (hemicalcium), and HEPES 20 mM) at 37 °C. To collect caput sperm, two small incisions were made at the proximal end of caput and using a 26G needle holes were poked in the rest of the tissue to let the caput epididymal fluid ooze out. For cauda sperm collection, cauda epididymis were gently squeezed to allow the caudal fluid to ooze out. Sperm-containing media was incubated for 15 minutes at 37 °C, then transferred to a fresh tube and the sperm-free epididymis tissues were directly frozen in liquid nitrogen and stored at -80 °C. The sperm were incubated for another 15 minutes at 37 °C, after incubation sperm were collected by centrifugation at 2000 x g for 2 minutes, followed by a 1X PBS wash, and a second wash with somatic lysis buffer (low or mid SLB, see below) for 10 minutes on ice to eliminate somatic cell contamination. Somatic lysis buffer treated sperm were collected by centrifugation at 3000xg for 5 minutes, and finally washed

with 1X PBS before freezing down. For caput sperm collection, somatic lysis buffer concentration or incubation time was increased if the sperm pellet appeared red (due to contaminating red blood cells). Sperm sample purity was confirmed by microscopic examination of the samples.

For testicular spermatocyte and spermatid isolation, testes were acquired from one mouse at 10-12 weeks of age and incubated without their tunica albuginea in 5 ml elutriation buffer (100 mM NaCl, 45 mM KCl, 6 mM Na₂HPO₄, 0.6 mM KH₂PO₄, 0.23% Sodium DL-Lactate, 0.1% Glucose, 0.1% BSA, 0.011% Sodium Pyruvate, 1.2 mM MgSO₄ and 1.2 mM CaCl₂) containing 25 µg/ml liberase TM (Roche Diagnostics GmbH) for 30 min at 37 °C with gentle agitation every 5 min to make cell suspension. The cell suspension was next pipetted 20 times with a 10-ml plastic pipette. After homogenization by pipetting 10 times through a P1000 pipette, the single cell suspension was filtered twice through a 40-µm cell strainer (Fisher Scientific) on ice and centrifuged at 1500 rpm at 4 °C for 10 min, and then the pellet was resuspended in 20 ml elutriation buffer. Next, testis cell populations were separated by centrifugal elutriation using a JE-5.0 elutriation system and a 4-ml standard elutriation chamber (Beckman Coulter). The system was assembled following the manufacturer's instruction. The precise elutriation conditions are as follows: Fractions 1-3 were run at 3000 rpm and fractions 4-5 were run at 2000 rpm. The flow rate was 14, 18, 31, 23, and 40 ml/min for fractions 1-5, respectively. Tubes from fractions 3 to 5 were spun at 1500 rpm at 4 °C for 10 min. Pellets from the same fraction were combined, resuspended in 200 µl of elutriation buffer and loaded onto 23-35% Percoll gradient, and centrifuged at 11,000 rpm at 4 °C for 15 min. The cells were then collected in 15-ml conical polypropylene tubes and spun at 1500 rpm at 4 °C for 15 min, and the pellets were stored at -80 °C. As described previously (Sharma et al., 2016), fraction 5 corresponds to primary spermatocytes and fractions 4 and 3 correspond to early and late round spermatids, respectively.

For mature testicular spermatozoa isolation, testes from one mouse (8-12 weeks old) were minced in a 35-mm Petri dish containing 1 ml 150 mM NaCl. Finely minced tissue slurry was then transferred to a 15ml conical tube and set aside for 3-5 minutes to allow tissue pieces to settle down. Next, the cell suspension was loaded onto 10.5 ml of 52% isotonic percoll (Sigma). The tubes were then centrifuged at 12000X g for 10 minutes at 10 °C. The pellet was resuspended in 10 ml of 150 mM NaCl and spun at 600X g at 4 °C for 10 minutes. The pellet was next washed with 75 mM NaCl solution 3 times, followed by treatment with somatic lysis buffer (0.01% SDS, 0.005% Triton-X) and one wash with 1X PBS to retrieve purified mature testicular spermatozoa. Spermatozoa pellets were then either flash frozen or used for fusion with epididymosomes.

Sperm Washing

Cauda epididymis were dissected from 8-12 week old FVB mice, placed in Whitten's media pH 7.4 (100 mM NaCl, 4.7 mM KCl, 1.2 mM KH₂PO₄, 1.2 mM MgSO₄, 5.5 mM Glucose, 1 mM Pyruvic acid, 4.8 mM Lactic acid (hemicalcium), and HEPES 20 mM), and gently squeezed at the distal end to allow the caudal fluid to ooze out into the media. Sperm containing media was incubated for 15 minutes at 37 °C, then transferred to a fresh tube and incubated for another 15 minutes at 37 °C. To ensure homogeneity of sperm samples undergoing varying concentrations of somatic lysis buffer (SLB) treatment, cauda sperm from multiple animals were pooled, mixed thoroughly and then re-divided into four tubes. Sperm were collected by centrifugation at 2000xg for 2 minutes, then washed with 1X PBS and spun down. Three of these tubes were treated with three different concentrations of somatic lysis buffer, namely, low SLB (0.01% SDS, 0.005% Triton-X), mid SLB (0.1% SDS, 0.005% Triton-X) and high SLB (0.1% SDS, 0.5% Triton-X) respectively, for 10 minutes on ice followed by centrifugation at 3000xg for 5 minutes. After one final wash with 1X PBS, the sperm pellet was obtained by centrifugation at 3000xg for 5 minutes, and flash frozen in liquid Nitrogen. The fourth sample was flash frozen right after the first PBS wash, without any somatic lysis. All sperm pellets were stored at -80 °C until RNA extraction.

Separation of Sperm Head and Tail

For the separation of cauda sperm head and tail, epididymides from one sexually mature mouse (12-15 weeks old) were slit open and sperm were gently squeezed out in a dish containing PBS. The dish was then incubated at 37 °C for 15 minutes. Sperm slurry from five such dishes were pooled into a 15 ml conical tube and incubated at 37 °C for another 15 minutes. Next, the supernatant was centrifuged at 1500x g for 15 minutes at 4°C and the cell pellet was either washed with cold 75 mM NaCl three times, or with somatic lysis buffer (0.01% SDS and 0.005% Triton X-100), to remove somatic cells followed by centrifugation at 4000x g for 5 minutes at 4°C. Purity of sperm preparations was confirmed by microscopic examination. The sperm pellet was resuspended in 5 ml mitochondrial wash buffer (0.25 M sucrose, 0.01 M Tris, 0.001 M EDTA, pH 7.4) and sonicated for 10 seconds at 4°C at setting 4 using a Sonifier cell disruptor, Model W185 (Heat System-Ultrasonic, Inc., Plainview, NY). The sonicate was layered over a discontinuous sucrose gradient containing 10 ml 0.9 M sucrose and 15 ml 2.0 M sucrose. The gradient was centrifuged at 10,000 rpm in a SW 28 rotor, at 10°C for 30 minutes. Sperm tails were collected from the interface of 0.9 M sucrose and 2.0 M sucrose, and the heads from the bottom of the tube. Heads and tails were then washed with TE buffer and PBS, flash frozen and stored at -80°C for later analysis.

For the separation of heads and tails from testicular spermatozoa, testes from one sexually mature mouse (12-15 weeks old) were gently minced in a 35 mm Petri dish containing 1 ml modified Whitten's media (22 mM HEPES, 1.2 mM MgCl₂, 100 mM NaCl, 4.7 mM KCl, 1.0 mM pyruvic acid, 5.5 mM glucose, 4.8 mM lactic acid, pH 7.3) and 1 mM PMSF. Minced tissue slurry from 13 mice was pooled into one 50 ml tube and set aside for 3- 5 minutes. The supernatant was layered over 30 ml 7.5% Percoll gradient and centrifuged at 1000x g for 20 minutes at 13 °C. The cell pellet was washed with cold 75 mM NaCl to remove somatic cells followed by centrifugation at 4000x g for 5 minutes at 4°C. The wash step was repeated three times. Next, the pellet was resuspended in 5 ml modified Whitten's media containing 1 mM PMSF and layered over 52% Percoll gradient, followed by centrifugation at 15,000 rpm in SW 28 rotor for 15 minutes at 10 °C. The pellet which contains purified testicular spermatozoa, was washed with

modified Whitten's media and sperm purity was examined by microscopic examination. Next, purified testicular spermatozoa were resuspended in 5 ml of mitochondrial wash buffer, sonicated, washed and flash frozen as described above for cauda sperm head/tail separation.

Epididymosome Isolation

Epididymosomes were isolated as previously described (Sharma et al., 2016). Briefly, caput epididymides were dissected from 8-12 weeks old male mice and placed in dishes containing 1 ml Whitten's media (100 mM NaCl, 4.7 mM KCl, 1.2 mM KH_2PO_4 , 1.2 mM MgSO_4 , 5.5 mM Glucose, 1 mM Pyruvic acid, 4.8 mM Lactic acid (hemicalcium), and HEPES 20 mM) pre-warmed at 37°C. The epididymides were then gently squeezed using forceps to isolate epididymal luminal content. The dishes containing epididymal luminal contents were then placed in an incubator set at 37°C with 5% CO_2 for 15 minutes, to allow any remaining epididymal contents to release from the tissue. Next, the media containing epididymal luminal contents was transferred to a 1.5 ml tube and allowed to incubate for an additional 15 minutes. At the end of the 15 minutes, any tissue pieces or non-motile sperm settled down at the bottom of the tube and all the contents of the tube except for the bottom ~50 μl were transferred to a fresh tube. Next, the tube was spun in a tabletop centrifuge at 2000x g for 2 minutes to pellet down sperm. Supernatant, which contains epididymosomes, was then transferred to a fresh tube and centrifuged at 10000x g for 30 minutes at 4°C to get rid of any non-sperm cells and cellular debris. Supernatant from this spin was then transferred to a polycarbonate thick wall tube (13 X 56 mm, Beckman Coulter, Catalog number 362305) and centrifuged at 100000x g for 2 hours at 4°C in a tabletop ultracentrifuge (Beckman Optima TL) using TLA100.4 rotor. The pellet from this spin was then washed with 500 μl 1X PBS and centrifuged for another 2 hours at 100000x g at 4°C. Finally, the pellet containing epididymosomes was resuspended in 50 μl ice-cold 1X PBS, transferred to a 1.5 ml tube and flash frozen in liquid nitrogen or used for fusion with sperm.

Testicular Spermatozoa and Caput Epididymosome Fusion

After final wash with 1XPBS, caput epididymosomes were resuspended in 62.5 μl media out of which 12.5 μl was flash frozen and 50 μl was used for fusion with testicular spermatozoa. For fusion reaction, purified 100 μl of testicular spermatozoa were mixed with 50 μl of caput epididymosomes in presence of 1 mM ZnCl_2 and incubated at 37°C for 2 hours. In parallel, a mock fusion reaction was also performed where no epididymosomes were added to the reaction. At the end of the incubation, additional 850 μl of 1X PBS was added to the reaction and sperm were spun down at 4000x g for 5 minutes. Next, the pellet was washed with 1X PBS three times and processed further for RNA extraction.

Two lines of evidence argue that gain of small RNAs in "reconstituted sperm" (Figure 4) results from epididymosomal RNA delivery to testicular sperm, rather than simple contamination by epididymosomes. First, initial reconstitution studies carried out with only one wash step resulted in a small RNA profile that almost perfectly matched the caput epididymosome RNA repertoire, demonstrating that the washes used in the final protocol removed excess epididymosomes. Second, the RNAs gained during reconstitution—dots above the diagonal in Figure 4E—are a subset of epididymosomal RNAs, consistent with a subset of RNAs being present in delivery-competent vesicles and again arguing against gross contamination of testicular sperm by the epididymosomal material.

PNK Treatment

Total RNA from testis, cauda epididymis or sperm (caput and cauda) was extracted as previously described (Sharma et al., 2016). Following gel purification of 18-40 nucleotide small RNAs and isopropanol precipitation, small RNAs were treated with T4 Polynucleotide Kinase (PNK)(NEB M0201) + T4 PNK reaction buffer, incubated at 37°C for 30 minutes followed by heat inactivation at 65°C for 20 minutes. Following enzymatic treatment an equal volume of Acid Phenol:Chloroform (Ambion) was added to purify the RNA by aqueous phase separation. Finally, RNA was isopropanol precipitated prior to small RNA cloning.

Small RNA Deep Sequencing

Isolation of 18-40 nts small RNAs was carried out as previously described (Sharma et al., 2016) by purification from 15% polyacrylamide-7M urea denaturing gels. The resulting small RNA was used for preparing sequencing libraries using the Small RNA TruSeq kit from Illumina (as per the manual). Small RNA sequencing data was analyzed as described previously (Sharma et al., 2016).

TaqMan Assays

Taqman assay quantitative RT-PCRs were performed as described previously (Sharma et al., 2016). Custom small RNA assays for tRF-VaI-CAC, tRF-GluCTC, tRF-GlyGCC and pre-designed microRNA assay for miR-34c, Let7c, Let7f and mir-10a were purchased from Life Technologies. U6 small nuclear RNA was used as an internal control to normalize small RNA levels in various sperm populations.

Note that values for cauda sperm in Figure 2B may be overestimated by ~4-fold, as Ct values for U6 were similar for testicular sperm and caput sperm, but were consistently 2 cycles higher in cauda sperm, suggesting that U6 decreases in abundance from caput to cauda sperm. In this case, using U6 for normalization would inflate the small RNA changes in cauda sperm, thereby accounting for the fact that all the RNAs assayed here appear to be ~4-fold more abundant in cauda sperm than expected from deep sequencing data, where for example miR-34c and let-7f levels are similar in cauda and testicular sperm. Regardless, our U6-normalized data are qualitatively highly concordant with our deep sequencing data, and strongly support the hypothesis that tRFs are indeed gained by sperm as they enter the epididymis.

Generation of Mice Expressing Tissue-Specific UPRT

To generate mice expressing tissue specific UPRT, we crossed homozygous CAGFPstopUPRT mice with either liver-specific *Albumin-cre* mice or caput epididymis specific *Defb41-cre* mice, to generate heterozygous [*Uprrt*^{-/+}, *Alb-Cre*] or [*Uprrt*^{-/+}, *Defb41-Cre*] mice, respectively. Since 4-thiouracil incorporation is sensitive to the levels of UPRT, we then backcrossed these mice with homozygous CAGFPstopUPRT mice to produce mice homozygous for *Uprrt* gene. Mouse genotyping was performed using quantitative PCR (qPCR) with DNA isolated from ear punches. For genotyping CAGFPstopUPRT mice, following primers and probes were used: 5'-ATT CCA AGA TCT GTG GCG TC-3' and 5'-CTT CTC GTA GAT CAG CTT AGG C-3' for mutant allele; 5'-CAC GTG GGC TCC AGC ATT-3' and 5'-TCA CCA GTC ATT TCT GCC TTT G-3' for wildtype allele; probe 5'-/Cy5/CCA ATG GTC GGG CAC TGC TCA A/Black Hole Quencher 2/-3' for wildtype allele and probe 5'-/6-FAM/CCG CAT CGG GAA AAT CCT CAT CCA/Black Hole Quencher 2/-3' for mutant allele. *Albumin-cre* mice were genotyped using: 5'-TTG GCC CCT TAC CAT AAC TG-3' for both wild-type and mutant allele, 5'-TGC AAA CAT CAC ATG CAC AC-3' for wildtype allele, and 5'-GAA GCA GAA GCT TAG GAA GAT GG-3' for mutant allele. Primers for *Defb41-cre* mice included: 5'-AGA TGC CAG GAC ATC AGG AAC CTG-3' and 5'-ATC AGC CAC ACC AGA CAC AGA GAT C-3' for transgene, 5'-CTA GGC CAC AGA ATT GAA AGA TCT-3' and 5'-GTA GGT GGA AAT TCT AGC ATC C-3' for internal positive control. The qPCR conditions were as follows: 95°C for 3 min, followed by 10 cycles of 95°C for 30 sec, 65°C for 15 sec, decrement of temperature by 0.5°C per cycle, 68°C for 10 sec, and 28 cycles of 95°C for 20 sec, 60°C for 20 sec, and 72°C for 15 sec, with a final extension at 72°C for 2 min.

4-Thiouracil (4-TU) Treatment

4-TU was dissolved in DMSO at 200 mg/ml and stored at -20°C. Prior to use, the stock solution was diluted at 1:4 with corn oil with rigorous shaking and working solution was then kept in dark. 8-12 weeks old adult mice were intraperitoneally injected with either 4-TU (400 mg/kg body weight) or solvent alone (control) every other day for 5 times, as sperm transits from caput to cauda epididymis in approximately 10 days. Tissue and sperm samples were collected (as described above) 5 hours after the last injection, flash frozen in liquid nitrogen and stored at -80°C until RNA extraction.

Northern and Dot Blot Analysis

We followed published method for dot blot analysis with some modifications (Rädle et al., 2013). In brief, equal amount of RNA (in binding buffer) from different experimental groups, was applied to Zeta membrane (Bio-Rad). A biotin-labeled DNA oligo was used as a positive control. The membrane was air-dried at room temperature for 5 minutes, followed by blocking at room temperature for 30 minutes with 10% SDS in PBS and 1mM EDTA. Next, the membrane was incubated in a solution containing 10% SDS in PBS and Streptavidin-HRP (Thermo Fisher Scientific) for 15 minutes at room temperature, followed by three washes with PBS containing SDS for 5 minutes each. After the final wash, biotinylated RNA were detected with Amersham ECL Western Blotting Reagent (GE Healthcare Life Sciences) using Amersham Imager 600 (GE Healthcare Life Sciences). For Northern blot analysis, 30 µg of RNA was denatured and run on a 15% acrylamide 7M urea gel, followed by transfer to a positively charged nylon membrane and UV-crosslinking. The membrane was next incubated with Streptavidin-HRP, washed and detected using ECL reagent, as above. For Northern blot analysis of tRNA fragments (Figure S5), we used the following probes: 3'tRF GlyGCC 5' TGCATTGGCCGGGAACC GAACCCGGGCTCCCGCG 3' and 3'tRF Val CAC 5' TGTTTCCGCCGGTTTCGAACCGGGGACCTTTCCGCG 3'

Western Blot

Protein extracts were prepared from mouse tissues using RIPA lysis buffer (150 mM sodium chloride, 1.0% NP-40, 0.5% sodium deoxycholate, 0.1% SDS, and 50 mM Tris, pH 8.0). Protein extracts were denatured with 2X Laemmli buffer (4% SDS, 10% 2-mercaptoethanol, 20% glycerol, 0.004% bromophenol blue, 0.125 M Tris-HCl, pH 6.8) at 95°C for 5 min and run on a 10% SDS-PAGE, followed by transfer to PVDF membrane. The membrane was next probed with anti-GFP (Invitrogen), anti-HA (Thermo Scientific) or anti-Actin (Thermo Scientific) antibodies at 1:1000 dilution followed by secondary antibody treatment at 1:2000 dilution (anti-mouse HRP and anti-rabbit HRP, Cell Signaling).

SLAM-Seq

4 µg of isolated total RNA was treated with 10 mM iodoacetamide under optimal reaction conditions (50 mM NaPi, pH8; 50% v/v DMSO; 15 min at 50°C). The reaction was quenched by addition of 10 mM DTT, followed by ethanol precipitation and small RNA library preparation as described previously (Jayaprakash et al., 2011). Briefly, total RNA was size selected (18-30 nt) by 15% denaturing polyacrylamide gel electrophoresis and subjected sequentially to 3' and 5' adapter ligation (employing linker oligonucleotides with four random nucleotides at the ligation interface to avoid ligation biases). Gel-purified ligation products were reverse transcribed using SuperScript III (Invitrogen) according to the manufacturer's instructions, followed by PCR amplification and high-throughput sequencing on an Illumina HiSeq 2000 instrument (SR100 mode).

QUANTITATION AND STATISTICAL ANALYSIS

For small RNA-Seq datasets, individual small RNA abundances were normalized to parts per million based on total number of reads mapping to microRNAs, tRNAs, piRNAs (repeatmasker and unique piRNAs), and mRNA (Refseq)—rRNA-mapping reads were excluded. Significant differences in small RNA abundance were calculated by t-test, adjusted for multiple hypothesis testing by

multiplying by the number of RNAs above an average abundance of 10 ppm. Complete genome mapping results for all small RNA-Seq datasets, with sample numbers, are available in [Tables S1, S2, S3, S4, and S5](#).

For the analysis of SLAM-seq datasets, small RNA reads were aligned using bowtie v.1.2 ([Langmead et al., 2009](#)), allowing for 3 mismatches, to all mouse pre-miRNA hairpins described in mirbase v.21 ([Kozomara and Griffiths-Jones, 2014](#)) and extended downstream by 20 basepairs. All reads mapping to 5p and 3p arms of a miRNA hairpin locus were filtered to only retain the most frequent 5' isoform. Mutation rates were determined by investigating the occurrence of any given mutation within the miR body (nt 1-18) of the most abundant miRNA 5' isoforms, normalized to the genome matching instances at this position and frequency of each nucleotide within the inspected region. Reads containing U>C conversions within the miR body were counted and normalized to U-content and total mapping reads to assess abundance in cpm. For any given sample, further analysis was restricted to microRNAs with at least 1000 reads.

Statistical significance for TU tracer experiments was assessed in two ways. For [Figures 5E and 6C](#), significant changes in U->C conversion rate were assessed across the entire set of detected microRNAs by paired two-tailed t-test, with Uninjected and TU-injected samples being paired for a given tissue. In addition, in [Figure S4D](#) we used KS tests to assess significance for the distribution of microRNAs exhibiting a given change in U->C conversion upon TU injection, comparing distributions in the testis vs. in cauda epididymal sperm. For TU tracer studies, n=2 animals, with each replicate set representing a sample of intact testis, intact caput epididymis, and cauda epididymal sperm obtained from the same animal.

DATA AND SOFTWARE AVAILABILITY

The accession number for the sequence data reported in this paper is GEO: GSE112990.